Cell Reports

Article

Pharmacological depletion of RNA splicing factor RBM39 by indisulam synergizes with PARP inhibitors in high-grade serous ovarian carcinoma

Graphical abstract

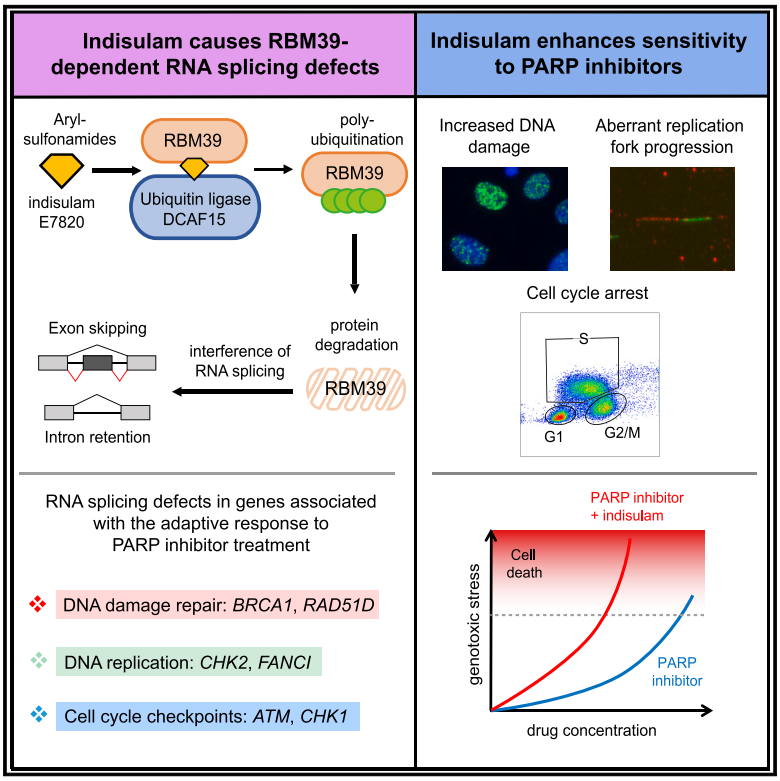

Highlights

- RBM39 regulates mRNA splicing of DNA damage repair genes such as *ATM* and *BRCA1*
- RBM39 depletion through indisulam synergizes with cisplatin and PARP inhibitors
- Olaparib-induced activation of ATM, Chk2, and Chk1 is suppressed by indisulam
- Indisulam improves response to olaparib treatment in a murine HGSC model

Authors

Yuewei Xu, Sarah Spear, Yurui Ma, ..., Iain McNeish, Hector C. Keun, Anke Nijhuis

Correspondence

h.keun@imperial.ac.uk (H.C.K.), a.nijhuis@imperial.ac.uk (A.N.)

In brief

Xu et al. show that RBM39 modulates correct splicing of various DNA damage repair factors in ovarian cancer cells. Depletion of RBM39 through molecular glues such as indisulam leads to RNA splicing defects in these genes and improves PARP inhibitor response *in vitro* and *in vivo*.

Xu et al., 2023, Cell Reports *42*, 113307
October 31, 2023
https://doi.org/10.1016/j.celrep.2023.113307

CellPress

Cell Reports

CellPress
OPEN ACCESS

Article

Pharmacological depletion of RNA splicing factor RBM39 by indisulam synergizes with PARP inhibitors in high-grade serous ovarian carcinoma

Yuewei Xu,[1] Sarah Spear,[1,2] Yurui Ma,[1] Marc P. Lorentzen,[1,2] Michael Gruet,[1] Flora McKinney,[1] Yitao Xu,[1] Chiharu Wickremesinghe,[1,2] Madelen R. Shepherd,[1] Iain McNeish,[1,2] Hector C. Keun,[1,2,*] and Anke Nijhuis[1,2,3,*]

[1]Department of Surgery & Cancer, Imperial College London, London, UK

[2]Ovarian Cancer Action Research Centre, Department of Surgery & Cancer, Imperial College London, London, UK

[3]Lead contact

*Correspondence: h.keun@imperial.ac.uk (H.C.K.), a.nijhuis@imperial.ac.uk (A.N.)

https://doi.org/10.1016/j.celrep.2023.113307

SUMMARY

Ovarian high-grade serous carcinoma (HGSC) is the most common subtype of ovarian cancer with limited therapeutic options and a poor prognosis. In recent years, poly-ADP ribose polymerase (PARP) inhibitors have demonstrated significant clinical benefits, especially in patients with BRCA1/2 mutations. However, acquired drug resistance and relapse is a major challenge. Indisulam (E7070) has been identified as a molecular glue that brings together splicing factor RBM39 and DCAF15 E3 ubiquitin ligase resulting in poly-ubiquitination, degradation, and subsequent RNA splicing defects. In this work, we demonstrate that the loss of RBM39 induces splicing defects in key DNA damage repair genes in ovarian cancer, leading to increased sensitivity to cisplatin and various PARP inhibitors. The addition of indisulam also improved olaparib response in mice bearing PARP inhibitor-resistant tumors. These findings demonstrate that combining RBM39 degraders and PARP inhibitors is a promising therapeutic approach to improve PARP inhibitor response in ovarian HGSC.

INTRODUCTION

Ovarian cancer is the deadliest gynecological cancer, with a 5-year survival rate of less than 50%.[1] Approximately 70% of ovarian cancer cases are high-grade serous carcinoma (HGSC), which accounts for the most ovarian cancer-related deaths.[2] The standard therapy for newly diagnosed ovarian cancer involves debulking surgery combined with carboplatin and paclitaxel chemotherapy. However, the disease often relapses with increased chemoresistance.[3]

Poly-ADP ribose polymerase (PARP) inhibitors have demonstrated significant clinical benefits in ovarian cancer patients with homologous recombination deficiency (HRD).[4] HRD can arise from deleterious mutations in *BRCA1/2* or loss of function in other key HR components, rendering cells unable to repair double-stranded DNA breaks (DSBs) accurately through HR repair.[5,6] By inhibiting PARP1/2-mediated repair of single-stranded DNA breaks (SSBs), PARP inhibitors achieve synthetic lethality in tumors with HRD.[7,8] Three PARP inhibitors—olaparib, rucaparib, and niraparib—have been approved for clinical use in subsets of ovarian cancer patients, demonstrating substantial benefits in delaying disease recurrence and improving overall survival.[9–13] However, approximately one-half of ovarian cancer patients are HR proficient and less responsive to PARP inhibitors.[5] Long-term administration of the drugs also leads to acquired PARP inhibitor resistance and reduced therapeutic response (reviewed in[14]). Additional interventions are therefore needed to improve PARP inhibitor response.

Splicing of precursor mRNAs (pre-mRNAs) is a critical regulatory step in gene expression, during which non-coding introns are spliced out from the final transcript. This process is mediated by the spliceosome, a dynamic protein-RNA complex consisting of splicing factors and small nuclear RNAs.[15–17] Pre-mRNAs of multi-exon genes can be spliced in several ways when alternative splice sites are recognized by splicing factors, generating mRNAs with different exon combinations, and subsequently translating to protein isoforms. Alternative RNA splicing diversifies the transcriptome and proteome and is fundamental to cell survival. However, dysregulated alternative splicing can promote tumorigenesis and chemoresistance.[18–22] In ovarian cancer, splicing factors are upregulated in at least 40% of cases,[23] and alternative splicing events have been associated with disease progression and patient prognosis.[24–30]

The RNA-binding protein RBM39 is a transcriptional co-regulator and splicing co-factor, and a promising therapeutic target in cancer (reviewed in[31]). Targeting RBM39 had been challenging until the recent discovery that RBM39 is selectively degraded by a panel of anticancer aryl sulfonamides, indisulam (E7070), E7820, chloroquinoxaline sulphonamide, and tasisulam.[32,33] These drugs act as molecular glues inducing a neo-interaction between RBM39 and DCAF15-associated E3-ubiquitin ligase complexes, resulting in poly-ubiquitination and proteasomal

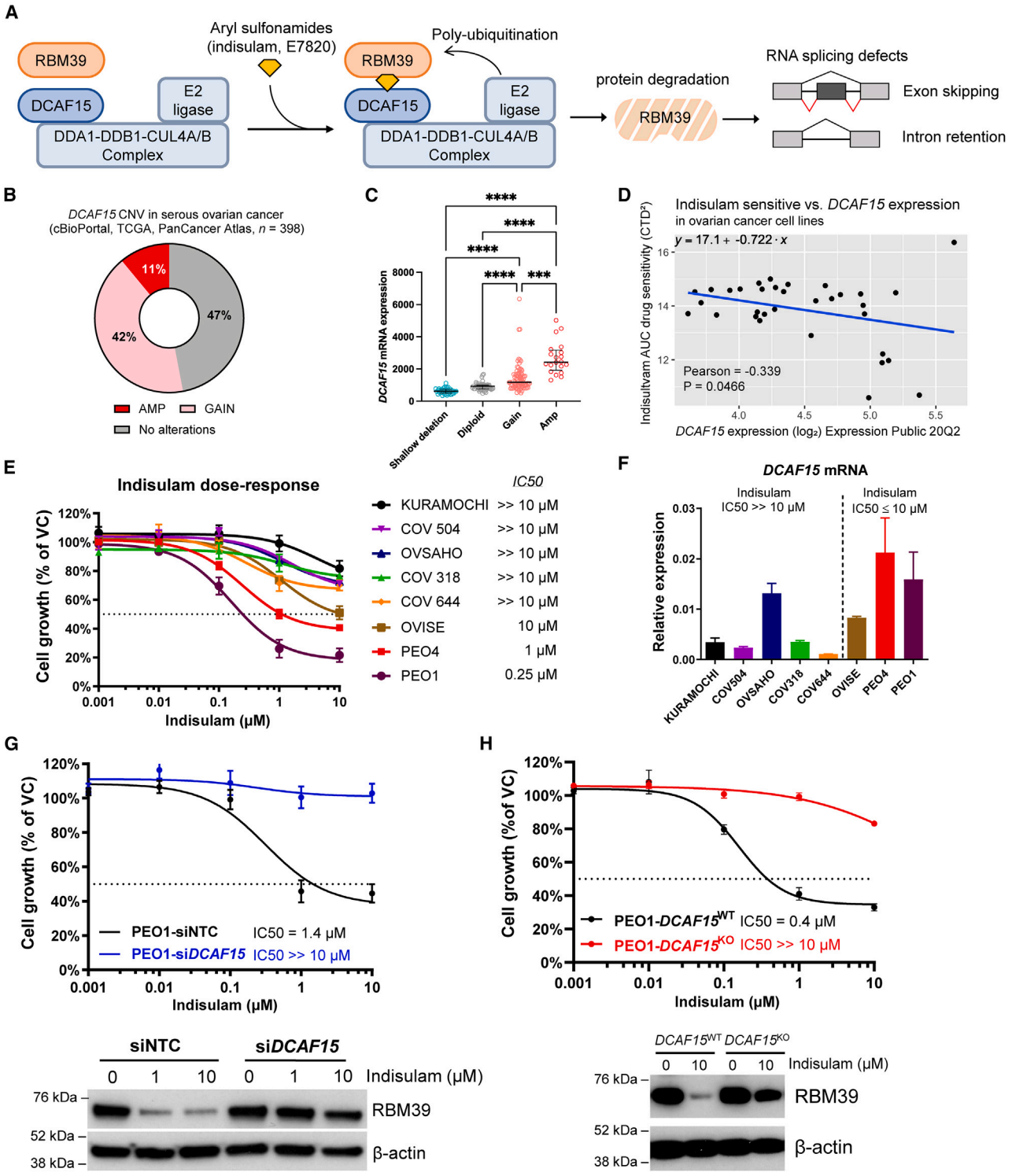

Figure 1. DCAF15 expression correlates to indisulam sensitivity in ovarian cancer cell lines

(A) Indisulam degrades RBM39 through a neo-interaction between RBM39 and DCAF15-associated E3 ubiquitin ligase. Loss of RBM39 disrupts the spliceosome and causes widespread splicing abnormalities. Diagram adapted from[31] with permission.

(B) Copy number variation (CNV) of *DCAF15* in serous ovarian cancer showed frequent amplification (AMP, n = 44) and gain of copy number (GAIN, n = 167). Data were extracted from The Cancer Gene Genome Atlas (TCGA) PanCancer Atlas on cBioPortal.[38,39]

(legend continued on next page)

degradation of RBM39.[32,33] Loss of RBM39 leads to transcriptome-wide splicing abnormalities and causes tumor regression in multiple cancer types, including lung cancer,[34] colorectal cancer,[32,34] acute myeloid leukemia,[35] and neuroblastoma,[36,37] but its impact on ovarian cancer has not been studied to date.

In our previous work,[36] we demonstrated that exposure to indisulam induces many aberrant splicing events affecting multiple DNA repair genes, suggesting that RBM39 may regulate these pathways. We hypothesized that RBM39 has similar functions in ovarian cancer and that targeting RBM39 may disrupt DNA repair pathways and improve PARP inhibitor response. In this work, we explored the therapeutic potential of RBM39 as a cancer target in ovarian cancer by investigating the impact of RBM39 depletion on splicing of DNA damage repair genes and introduce PARP inhibitor in combination with indisulam as a promising strategy. In addition, we characterize the combination therapy from the perspectives of DNA damage repair, replication stress, and *in vivo* tumor growth.

RESULTS

Indisulam causes RBM39 degradation in ovarian cancer

Small molecular glue aryl sulfonamides generate new protein-protein interactions between RBM39 and E3 ubiquitin ligase DCAF15 (Figure 1A). *DCAF15* expression is required for RBM39 degradation and cytotoxicity,[32,33] and thus the expression in tumors is an important factor. Copy number gain or amplification of *DCAF15* was observed in 53% of HGSC in The Cancer Gene Genome Atlas,[38,39] which correlated with upregulated mRNA expression (Figures 1B and 1C). Drug sensitivity from the Cancer Target Discovery and Development[2] Network[40–42] demonstrated *DCAF15* expression levels in ovarian cancer cell lines positively correlated with indisulam sensitivity ($p = 0.0466$), which is consistent with findings in other cancer types[32,33,35–37] (Figure 1D). This association was confirmed *in vitro* in ovarian cancer cells (except for OVSAHO): cells with higher *DCAF15* expression were more sensitive to indisulam (Figures 1E and 1F), and indisulam caused a dose-dependent degradation of RBM39 (Figure S1). Knockdown (via small interfering RNA) or knockout (via CRISPR-Cas9) of *DCAF15* in PEO1 cells conferred resistance to indisulam and rescued indisulam-mediated RBM39 degradation and (Figures 1G and 1H) and RNA splicing (Figure S1C), implying that DCAF15-mediated RBM39 degradation is necessary for efficacy. Interestingly, even in the most resistant cell line, KURAMOCHI, indisulam was able to degrade RBM39 (Figure S1B), despite a low level of basal *DCAF15* mRNA expression relative to other ovarian cancer cells. This indicates that cell dependency on RBM39, besides DCAF15 levels, may determine response to indisulam. Taken together, our data demonstrate that indisulam inhibits ovarian cancer proliferation by depleting RBM39, and that *DCAF15* expression is likely necessary but not sufficient to predict indisulam cytotoxicity.

RBM39 regulates the splicing of DNA damage repair genes

Transcriptome-wide characterization of alternative splicing events after RBM39 depletion has been investigated in multiple cancer types, but not in ovarian cancer. Although there could be cancer-specific differences, we speculate that RBM39 modulates a robust RNA splicing signature across various cancer types. To identify common alternative splicing targets of RBM39, we analyzed 11 publicly available RNA sequencing datasets with alternative splicing analysis in RBM39-depleted cancer cells. These include five datasets in neuroblastoma cells (BE2C and SKNAS),[37] three melanoma cells (501-MEL-ES, A375, and SK-MEL-239),[43] two in acute myeloid leukemia cells (MOLM-13 and THP-1),[35] and one in MCF-7 breast cancer cells[44] (Figures S2A–S1B). These datasets were analyzed in combination with our recently published splicing analysis in neuroblastoma.[36] We found that, upon RBM39 depletion, exon skipping events in 1,774 genes and intron retention in 629 genes were repeatedly detected in at least 6 cell lines and where at least 2 of these lines were from different cancers (Table S1). Pathway enrichment analysis revealed that cell-cycle and DNA repair pathways are preferential splicing targets of RBM39, indicating a consistent role of RBM39 in modulating genes in cell-cycle and DNA damage repair response pathways (Figure S2C).

To investigate the impact of RBM39 depletion with indisulam in ovarian cancer, we performed RNA sequencing and alternative splicing analysis in KURAMOCHI using two commonly used algorithms, Splicefisher[32] and rMATS.[45] These analyses revealed that indisulam increased RNA splicing events compared with controls, mainly generating exon skipping events and intron retention events (Figures 2A and S2D). These genes were highly enriched for pathways related to RNA metabolism, cell cycle, and DNA damage repair (Figures 2B and S2F). Notably, indisulam caused aberrant splicing events in many DNA repair genes, such as *ATM*, *ATR*, Fanconi anemia genes (*FANCI*), HR genes

(C) Amplification (n = 20) or gain of *DCAF15* (n = 85) correlates with increased mRNA expression in serous ovarian cancer (shallow deletion, n = 40; diploid, n = 56). Kruskal-Wallis test and Dunn's multiple comparisons test were used for statistical analysis (***$p < 0.001$, ****$p < 0.0001$).

(D) Higher *DCAF15* expression was associated with increased sensitivity to indisulam (area under the curve [AUC]). Data were downloaded from DepMap portal (https://depmap.org/portal/) and a total of 33 cell lines were analyzed.

(E) Human ovarian cancer cell lines were treated with increasing doses of indisulam for 72 h and cell growth was measured by SRB assay (n = 3, independent experiments). The concentration causing 50% growth inhibition was defined as the median inhibition concentration (IC50).

(F) mRNA level of *DCAF15* in ovarian cancer cell lines was quantified using real-time PCR (n = 3). ΔCt, the difference between cycle threshold values from real-time PCR.

(G) PEO1 cells transfected with *DCAF15* small interfering RNA (siRNA) (siDCAF15) or non-targeting control (siNTC) before measuring indisulam sensitivity using the sulforhodamine B assay (SRB) (top) (n = 3) and RBM39 degradation (bottom) (6-h treatment) (n = 3).

(H) PEO1 cells were edited with CRISPR-Cas9 to generate *DCAF15* knockout clones (PEO1-*DCAF15*^{KO}) and mock editing clones (PEO1-*DCAF15*^{WT}). Cell growth (n = 3) and RBM39 degradation (48 h, n = 3) in these clones were investigated using SRB and western blot, respectively. Dashed lines in (E), (G), and (H) indicate 50% growth inhibition. All data are mean ± SEM. VC, vehicle control. See also Figure S1.

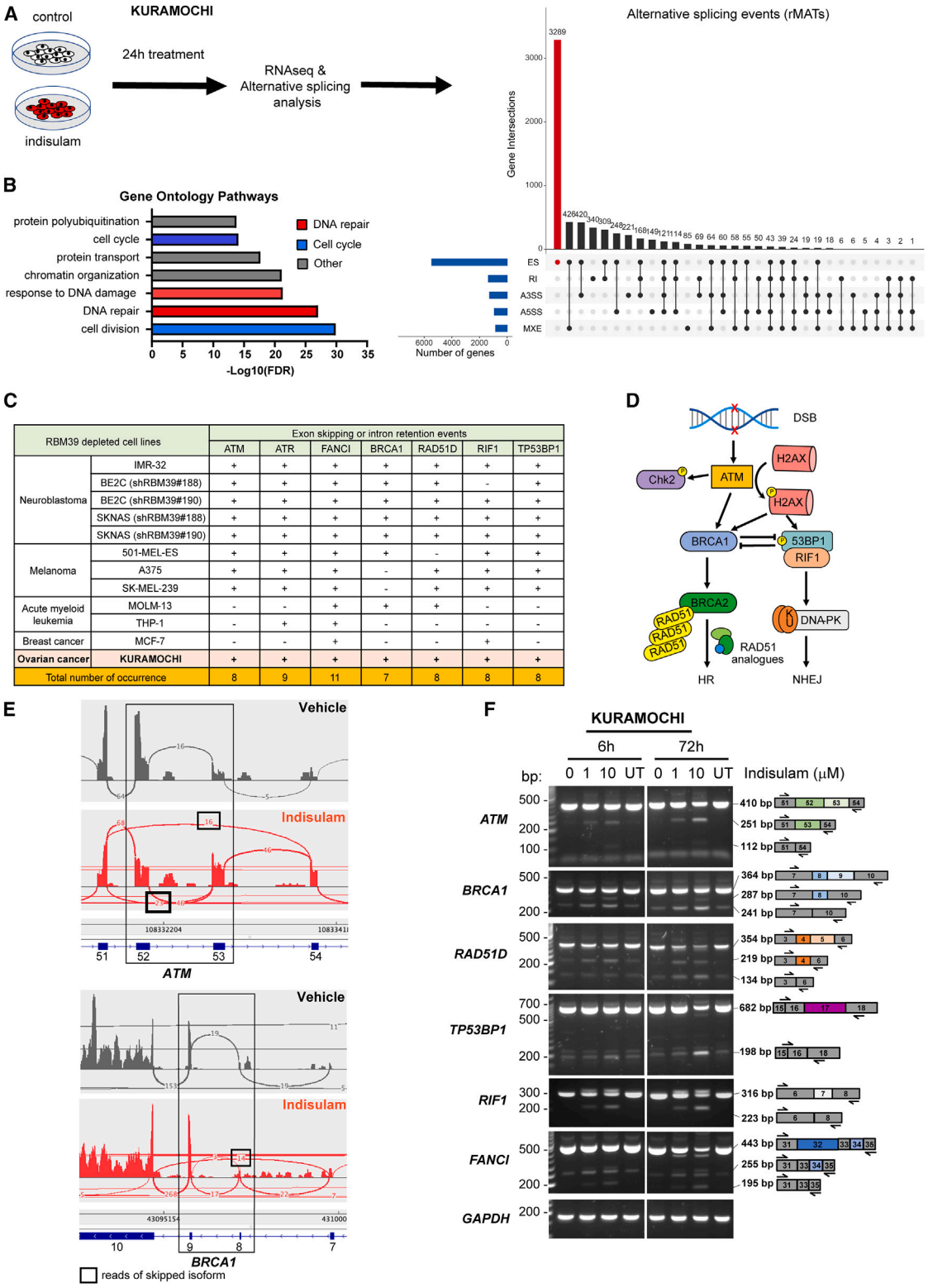

RBM39 depleted cell lines		Exon skipping or intron retention events						
		ATM	ATR	FANCI	BRCA1	RAD51D	RIF1	TP53BP1
Neuroblastoma	IMR-32	+	+	+	+	+	+	+
	BE2C (shRBM39#188)	+	+	+	+	+	-	+
	BE2C (shRBM39#190)	+	+	+	+	+	+	+
	SKNAS (shRBM39#188)	+	+	+	+	+	+	+
	SKNAS (shRBM39#190)	+	+	+	+	+	+	+
Melanoma	501-MEL-ES	+	+	+	+	-	+	+
	A375	+	+	+	-	+	+	+
	SK-MEL-239	+	+	+	-	+	+	+
Acute myeloid leukemia	MOLM-13	-	-	+	+	+	-	-
	THP-1	-	+	+	-	-	-	-
Breast cancer	MCF-7	-	-	+	-	-	+	-
Ovarian cancer	**KURAMOCHI**	+	+	+	+	+	+	+
Total number of occurrence		8	9	11	7	8	8	8

Figure 2. RBM39 depletion causes splicing errors in DNA damage repair genes

(A) Workflow for indisulam treatment in KURAMOCHI. UpSet plot depicting alternative splicing events (ASE) as determined by rMATS (24 h) (n = 3 independent experiments). Bars represent number or events per splicing event type with dots indicating intersections between events for the number of genes. One gene may

(legend continued on next page)

(*BRCA1* and *RAD51D*), and non-HR (i.e., non-homologous end-joining) (*TP53BP1* and *RIF1*) (Figures 2C and 2D). Alternative splicing of these DNA repair genes is also affected in other cancer types (Figure 2C), suggesting a conserved role for RBM39 in regulating the alternative splicing of key players in the response to DNA damage.

To validate the changes in splicing at the RNA level, we used PCR with custom-made primers flanking the affected exons of *ATM*, *BRCA1*, *RAD51D*, *TP53BP1*, *RIF1*, and *FANCI*, which permits the detection of exon skipping events. PCR analysis showed that indisulam exposure results in aberrant splicing in these genes (Figures 2E, 2F, and S3), potentially leading to truncated variants that are unlikely to translate to functional proteins because of frameshifts or deletions in functional domains. For example, skipping of exons 52 and 53 in *ATM* mRNAs is likely to disrupt the catalytic activity of ATM caused by deletions (aa. 2544–2642) in the kinase domain.[46,47] The splicing variants of *ATM* lacking exon 53 (139 bp), *BRCA1* lacking exon 9 (77 bp), and *TP53BP1* lacking exon 17 (484 bp) are expected to produce frameshifts and premature stop codons, potentially leading to nonsense-mediated decay.[48]

Overall, our findings demonstrate that RBM39 depletion modulates the splicing of DNA repair genes across multiple cancer types, including ovarian cancer. Targeting RBM39 may create vulnerabilities in cancer cells to anticancer drugs that increase genotoxic stress.

Indisulam synergizes with cisplatin and PARP inhibitors in ovarian cancer

Since indisulam induces splicing errors in DNA damage repair genes, we speculated that this may disrupt DNA damage response and render ovarian cancer cells more susceptible to DNA damaging agents, such as platinum-based chemotherapy, or agents that target DNA repair, such as PARP inhibitors, both of which are routinely used in ovarian cancer treatment. KURAMOCHI and OVSAHO cells were tested as these lines most closely represent ovarian HGSC,[49] and are intrinsically resistant to cisplatin and PARP inhibitors compared with other HGSC models that also present with loss of BRCA1/2 (i.e., PEO1) (Figures 3A, 3B, and S4). BRCA1/2 loss is generally associated with HR deficiency and synthetic lethality with PARP inhibitors.[7,50]

Combination index values calculated with the Chou-Talalay method[51] demonstrated that the combination of indisulam and cisplatin synergistically inhibited growth of KURAMOCHI and OVSAHO cells (Figure 3C). Furthermore, we observed that indisulam, even at doses not causing apoptosis, sensitized KURAMOCHI and OVSAHO cells to cisplatin-induced cell apoptosis (Figure 3C), adding to the evidence of synergism between these two treatments.

To test whether indisulam improves PARP inhibitor response in ovarian cancer cells, we combined indisulam with clinical PARP inhibitors olaparib, rucaparib, veliparib, or niraparib in a panel of human ovarian cancer cell lines (Figures 3D and S5). Synergistic interactions were observed in almost all drug combinations and all cell lines regardless of drug sensitivity, *BRCA* mutational status, or the differential PARP trapping capacity[52–55] of the PARP inhibitors tested (Figures 3D, S4, and S5). Subsequent assays validated that combination therapy of indisulam and olaparib caused synergistic growth inhibition and cell apoptosis in KURAMOCHI and OVSAHO cells (Figure 3E). Flow cytometry analysis further demonstrated that the Annexin V+/PI + population induced by the drug combination could be rescued by the pan-caspase inhibitor Z-VAD-FMK, confirming apoptosis as the major form of cell death (Figures 3F and 3G). In addition, a short-term exposure (48 or 72 h) to indisulam and olaparib in combination was sufficient to induce a synergistic and long-lasting inhibitory effect on HGSC colony growth (at least 9 days after drug removal) (Figure S6), a desirable characteristic for future clinical translation.

Exon skipping events of DNA repair genes, such as *ATM* and *TP53BP1*, were also confirmed in cells treated with indisulam alone and in combination with olaparib (Figure S7). Furthermore, CRISPR-Cas9 knockout of *DCAF15* completely abolished the synergistic interaction between indisulam and olaparib, suggesting that DCAF15-mediated RBM39 degradation and subsequent splicing events are necessary for this interaction (Figure 3H). This is consistent with the fact that E7820, another molecular degrader of RBM39 via DCAF15, also acts in synergy with olaparib (Figure S8).

Interestingly, a synergistic interaction between indisulam and olaparib was observed in both BRCA2-mutated PEO1 cells and in patient-matched PEO4 cells obtained at the point of clinical relapse (Figure S9A). PEO4 cells are known to possess a reversion mutation in BRCA2 that partially restores HR capacity and is associated with clinical resistance to platinum.[56,57] This supports our observations in other lines (Figures 3D, S4, S5, and S9B) that BRCA status does not predict if a synergistic benefit will occur. It also provides a potential rationale for using the combination in HGSC patients regardless of HRD status, including using indisulam to re-sensitize to chemotherapy agents in tumors that have become resistant because of reversion events in *BRCA*.

Taken together, our findings demonstrate that combining indisulam or other RBM39-targeting molecular glues with PARP inhibitor treatment is a promising strategy to target HGSC

undergo multiple splicing event types. The most common event is ES. ES, exon skipping; RI, retained intron; A3SS, alternative 3′ splice site; A5SS, alternative 5′ splice site; MXE, mutually exclusive exon.

(B) Pathway enrichment analysis (false discovery rate [FDR] <0.1) using Gene Ontology on intron-retained or exon-skipped genes (from rMATS analysis).

(C) Meta-analysis of 11 alternative splicing datasets in RBM39-depleted cells, including our datasets in KURAMOCHI and IMR-32.[36] Common key damage repair genes are depicted. +, genes exon skipped or intron retained; –, no exon skipping or intron retention events detected.

(D) A simplified diagram highlighting the role of ATM, BRCA1, RAD51 analogous, 53BP1, and RIF1 in DSB repair.

(E) Sashimi plots of exon skipping events in *ATM* (exons 52 and 53) and *BRCA1* (exons 8 and 9) in KURAMOCHI following indisulam exposure. Read counts of exon skipped splicing variants are highlighted in bold boxes.

(F) PCR validation of indisulam-induced exon skipping events in DNA repair genes (n = 4 technical replicates across four timepoints). *GAPDH* was included as a control. UT, untreated. See also Figures S2 and S3.

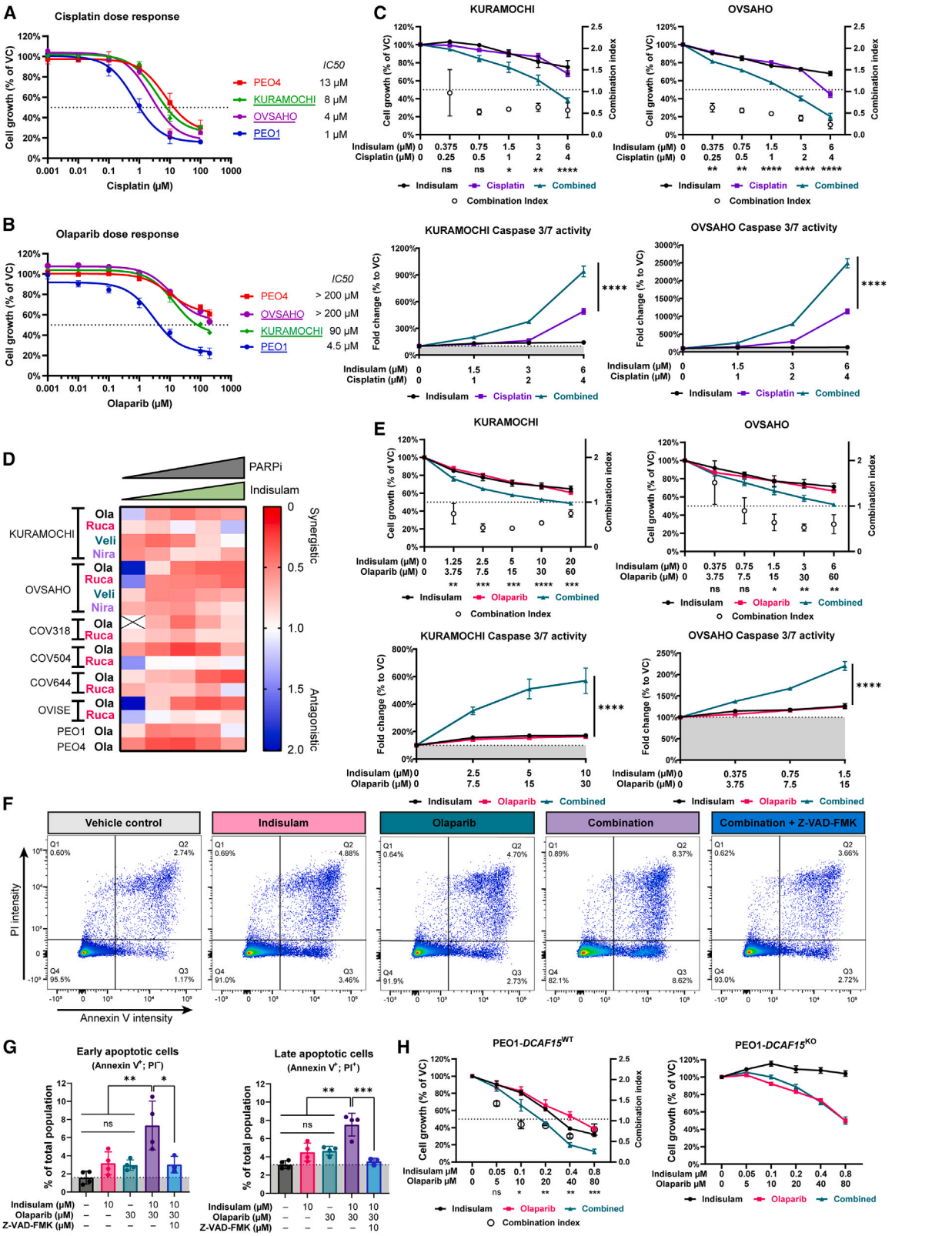

(legend on next page)

cells. Our observations are consistent with our hypothesis that indisulam may render cells more vulnerable to therapies causing DNA damage or targeting DNA repair through mis-splicing of genes involved in DNA damage response and repair pathways.

Indisulam treatment exacerbates genotoxic stress caused by olaparib

PARP inhibitors increase genotoxic stress by inducing DNA damage (SSBs and DSBs) and promote replication fork abnormalities.[58] The ATM-Chk2-mediated DNA damage repair and the ATR-Chk1-mediated replication stress response are two mechanisms that promote cancer cell survival in response to PARP inhibitor treatment.[59–62]

Since indisulam-mediated RBM39 degradation induces aberrant splicing errors in ATM and downstream DNA repair genes, we hypothesized that indisulam sensitizes ovarian cancer cells to PARP inhibitors by suppressing ATM-mediated DNA damage response. Western blot analysis in KURAMOCHI revealed that indisulam decreased ATM protein expression and suppressed olaparib-induced phosphorylation of ATM (pATM-S1981) and Chk2 (pChk2-T68),[63] indicating that indisulam impaired the ability to mount a DNA damage response (Figure 4A). We assessed the level of DNA damage with phosphorylated H2AX (γ-H2AX), which increases in response to DSBs[64,65] and stalled replication forks.[65–70] While monotherapy of indisulam or olaparib had a minor impact on γ-H2AX expression, combination therapy led to a substantial increase, a consequence of DSBs or replication stress (Figure 4A). Similarly, immunofluorescence analysis of foci demonstrated that indisulam and olaparib potentiate γ-H2AX foci formation (Figures 4B and S10A), which was also observed when indisulam was combined with other PARP inhibitors (Figure S10B-G).

Flow cytometry analysis in KURAMOCHI following treatment with indisulam and olaparib were more likely to arrest in S phase (mean = 53.8%, $p < 0.01$) compared with indisulam (mean = 38.5%) or olaparib (mean = 42.9%) alone (Figures 4C and 4D). Interestingly, cells treated with the combination therapy had the least nucleotide incorporation (mean = 47% of vehicle control) (Figure S11A), which suggests reduced DNA synthesis. This is in line with a reduction in levels of total and phosphorylated (S345) Chk1 (Figure 4A). Chk1 safeguards DNA replication by restarting stalled replication forks and inhibits unscheduled new origin firing.[71–75] Therefore, we hypothesized that the combination of indisulam and olaparib might cause DNA replication abnormalities. To this end, we examined DNA replication fork behaviors using DNA fiber analysis. While indisulam or olaparib alone had minor to moderate impacts on the length of newly synthesized DNA (DNA fibers), their combination led to significantly shorter DNA fibers, indicating increased fork stalling or reduced fork restarting (Figures 4E and 4F). Finally, combination therapy led to a profound increase in new origin firing (Figures S11B and S11C), which is consistent with the effect of Chk1 inhibition.[71,76,77]

Taken together, our data indicate that indisulam increases PARP inhibitor response by exacerbating genotoxic stress, with concomitant suppression of the ATM-Chk2-mediated DNA damage repair and Chk1-modulated replication stress response.

Combination of indisulam and olaparib demonstrates significant survival benefits *in vivo*

Next, we evaluated the combination of indisulam and olaparib in a well-characterized mouse model of ovarian HGSC (ID8).[78,79] This model recapitulates the process of peritoneal metastasis and development of ascites, observed in ovarian HGSC patients, and mimics the tumor immune microenvironment, which is advantageous over traditional xenografts (Figure 5A).[78] Pilot studies were conducted to determine maximal tolerable doses and optimal dosing schedules of indisulam and olaparib; additional adverse effects were not observed when both drugs were combined (Table S2). Daily intraperitoneal administration of up to 15 mg/kg of indisulam and 50 mg/kg of olaparib for 11 days were well tolerated and used for survival analyses (Figure 5B). In comparison with mice receiving vehicle control (median survival = 47 days), olaparib treatment alone only offered moderate survival benefits (median survival = 56 days; $p = 0.0206$) while indisulam alone improved the median survival to 65 days ($p = 0.0063$) (Figure 5C). Further, the combination of indisulam and olaparib resulted in the longest survival and was significantly more effective than olaparib monotherapy (median survival = 73 days; $p = 0.0041$). Of note, one of the mice in the

Figure 3. Indisulam improves cisplatin and PARP inhibitor response in ovarian cancer cells

(A and B) Growth assay (SRB) of four ovarian HGSC cell lines (PEO1, PEO4, KURAMOCHI, and OVSAHO) treated with increasing doses of cisplatin (A) and olaparib (B) for 72 h (n = 3 independent experiments, PEO4; cisplatin, n = 2). Cell lines with *BRCA2* mutation or deletions are underlined.

(C) Cell growth and apoptosis in KURAMOCHI and OVSAHO cells treated with indicated doses of indisulam and cisplatin either alone or in combination (n = 3 independent experiments). Open circles indicate combination index (CI) values (right y axis).

(D) Heatmap of CI values of indisulam in combination with indicated PARP inhibitors (PARPi) in a panel of human ovarian cancer cell lines. The square with a cross indicates no CI value could be calculated.

(E) Cell growth and apoptosis of KURAMOCHI and OVSAHO cells after treatment of indisulam, olaparib, or combination (n = 3 independent experiments). Open circles indicate CI values (right y axis)

(F) KURAMOCHI cells exposed to indisulam and olaparib individually or in combination (with or without 10 μM Z-VAD-FMK) for 48 h. Apoptosis was analyzed by flow cytometry using dual labeling of Annexin V and propidium iodide (PI). Data from a representative experiment are shown here.

(G) Quantification of early apoptotic (Annexin V^+ and PI^-) and late apoptotic cells (Annexin V^+ and PI^+) from flow cytometry analysis in (F). Ordinary one-way ANOVA analysis and Tukey's multiple comparison tests were used for statistical analysis ($n \geq 3$).

(H) Growth assay of PEO1-*DCAF15*^{WT} and PEO1-*DCAF15*^{KO} cells treated with indisulam and olaparib either alone or in combination for 72 h (n = 3 independent experiments). Open circles indicate CI values (right y axis). Statistical significance between drug combination and individual treatment (C, E, G, and H) was determined by two-way ANOVA and Dunnett's multiple comparisons test. ns, not significant, $^*p < 0.05$, $^{**}p < 0.01$, $^{***}p < 0.001$, $^{****}p < 0.0001$. CI values lower than 1 indicate synergism and CI values larger than 1 indicate antagonism (error bars indicate ±SD). Data indicate mean ± SEM (A–C, E, and H) or ±SD (G). VC, vehicle control. See also Figures S4, S5, and S6.

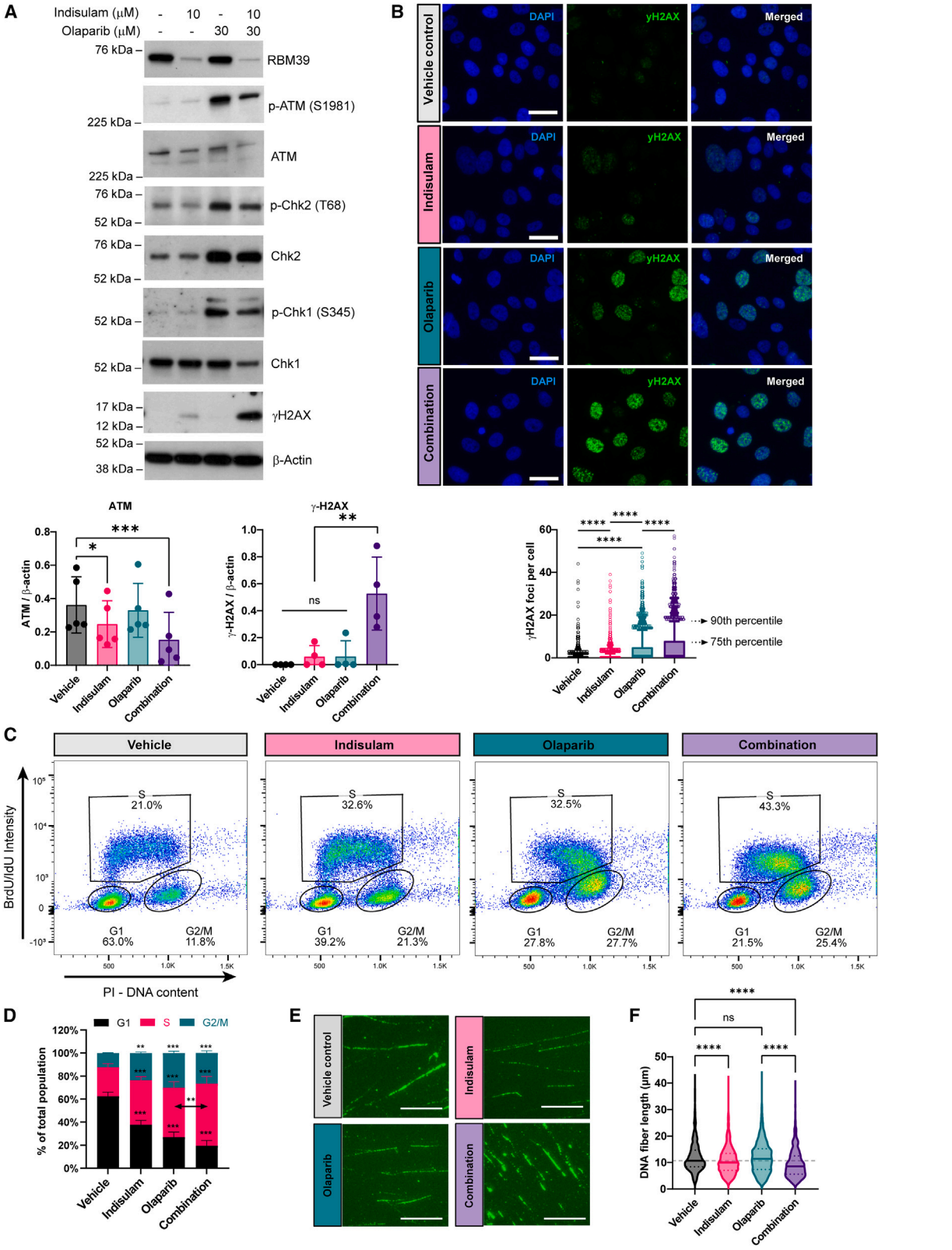

(legend on next page)

combination group survived until the end of the study (120 days) and showed complete tumor regression (Figure 5C).

Western blot analysis of the omental tumor deposits exposed to combination therapy indicated a dose-dependent degradation of Rbm39 confirming the on-target effect of indisulam (Figures 5D and 5E). Reduction of Atm and accumulation of γ-H2AX were also observed in tumor tissues following simultaneous administration of indisulam and olaparib, which is consistent with *in vitro* observations (Figures 5D and 5E). In summary, these data demonstrate that indisulam improves olaparib response in HR-proficient ovarian cancer *in vivo*, highlighting the promising therapeutic value of indisulam to expand the clinical use of PARP inhibitors in ovarian HGSC.

DISCUSSION

Ovarian HGSC is a leading cause of gynecologic cancer-related death, with limited options for targeted therapies.[2,80–82] Routine administration of PARP inhibitors has led to the emergence of drug resistance, despite promising benefits of delaying disease relapse and improving the overall survival of ovarian cancer patients.[83] PARP inhibitor resistance can occur in multiple ways with reversion mutations that restore HR proficiency a common observation in the clinic.[14]

Our systematic literature and transcriptomic analysis uncovered the role of RBM39 in coordinating RNA splicing of cell-cycle and DNA damage repair genes in various cancer cells. Using a variety of functional assays, we show that RBM39-degrading molecular glues such as indisulam can be repurposed as a therapeutic agent to improve PARP inhibitor response *in vitro* and *in vivo*. Importantly, a synergistic interaction between indisulam and various PARP inhibitors was observed in multiple ovarian HGSC cell lines *in vitro*, including BRCA-mutated and PARP inhibitor-sensitive cell lines (PEO1 and ID8-*Trp53*$^{-/-}$;*Brca2*$^{-/-}$) and PARP inhibitor-resistant cell lines (KURAMOCHI, OVSAHO, PEO4, COV318, COV504, COV644, and ID8-*Trp53*$^{-/-}$). The synergy seems to be *DCAF15* dependent and can be recapitulated when indisulam was substituted with E7820, a second RBM39 degrader. These findings suggest that previously reported off-target effects of indisulam, such as carbonic anhydrases inhibition or *DCAF15*-independent metabolic changes,[36,84–86] do not contribute to the observed synergy. Notably, in *Brca1/2*-wildtype ID8 cells (ID8-*Trp53*$^{-/-}$), the combination of indisulam and olaparib offered greater survival benefits than either monotherapy, demonstrating that indisulam improves PARP inhibitor response in mice with PARP inhibitor-resistant ovarian tumors. Further, our findings are consistent with a recent CRISPR-dropout screen, where *RBM39* knockout sensitized cells to olaparib treatment or PARP1 knockout.[87] Importantly, some of the downstream mis-spliced events following RBM39 loss, such as various Fanconi anemia genes (FANCA, FANCI, FANCL, and FANCM), are also negative determinants of response to PARP inhibitors.[88–91]

Mechanistically, indisulam disrupts RBM39-mediated splicing of the cell cycle, DNA damage repair, and DNA replication genes, leading to decreased protein expression and a defective adaptive response to genotoxic stress caused by PARP inhibitors. Indisulam decreased ATM expression at the protein level, which is likely due to splicing errors causing frameshifts in the open reading frame. Indisulam-mediated ATM downregulation has also been documented in neuroblastoma cells,[37] but the authors did not go on to investigate functional consequences. We show that indisulam suppresses olaparib-induced activation of ATM-Chk2-mediated DNA damage response and Chk1-mediated replication stress response, associated γH2AX accumulation, increased replication fork abnormalities, cell-cycle arrest in S phase, and cell apoptosis. These phenotypes are similar to those observed with a combination of PARP inhibitor and ATM inhibitors[92,93] or inhibitors targeting Chk1 or Chk2.[94–96]

An intriguing observation in this study was that the combination of indisulam and olaparib, but not monotherapies, decreased Chk1 expression. PARP1 has been implicated in pre-mRNA splicing,[97–100] and it is possible that simultaneous disruption of PARP1- and RBM39-mediated RNA splicing affected the expression of genes such as Chk1. Alternatively, RBM39 may interact directly or indirectly (through other splicing factors) with PARP1 as PARP1 was co-immunoprecipitated with RBM39,[35] and both interact with the core splicing factor SF3B1.[97,101] Additional transcriptomic and RNA splicing analysis of combination therapy would shed light on further processes contributing to drug-drug interactions, including modulation of RNA splicing by PARP1 inhibition.

Indisulam was discovered as a cell-cycle inhibitor in the late 1990s,[102] but its mechanism of action was only revealed by two seminal studies in 2017.[32,33] Aryl sulfonamides like indisulam are now recognized as a novel class of molecular glues

Figure 4. Indisulam inhibits ATM expression and exacerbates genotoxic stress caused by PARP inhibitors

(A) Western blot analysis (top) and densitometry analysis (bottom) of proteins of KURAMOCHI cells after 48 h treatment of indicated drugs (representative blot from n > 3 independent experiments). One-way ANOVA and Dunnett's multiple comparison test were used to determine the statistical significance.

(B) Immunofluorescence of KURAMOCHI cells treated with indisulam or olaparib as monotherapies or in combination for 24 h (top; representative image of n = 3 independent experiments). Analysis of γ-H2AX foci from three independent experiments (bottom; whiskers indicate 10th and 90th percentiles). Size bar, 50 μm.

(C) Flow cytometry-based cell cycle profiling of KURAMOCHI cells after 48 h treatment of 10 μM indisulam, 30 μM olaparib, or the combination. Cellular DNA content was labeled with propidium iodide (PI) and replicating cells were labeled with nucleotide analogues 5-bromo-2′deoxyuridine (BrdU) and 5-iodo-2-deoxyuridine (IdU).

(D) Analysis of cell cycle analysis (n = 3 independent experiments). Two-way ANOVA and Tukey's multiple comparisons test were used to determine statistical significance among groups.

(E) DNA fiber analysis quantifying replication fork behaviors in KURAMOCHI cells after 48 h exposure to indisulam, olaparib, or combination. Representative fields are shown. Scale bar, 20 μm.

(F) Violin plots (with median and interquartile range) of DNA fiber length measurements (at least 300 fibers from 2 independent experiments). Kruskal-Wallis test and Dunn's multiple comparisons test were used to determine statistical significance. Ns, not significant, *p < 0.05, **p < 0.01, ***p < 0.001, ****p < 0.0001. All data are mean ± SD. See also Figures S10 and S11.

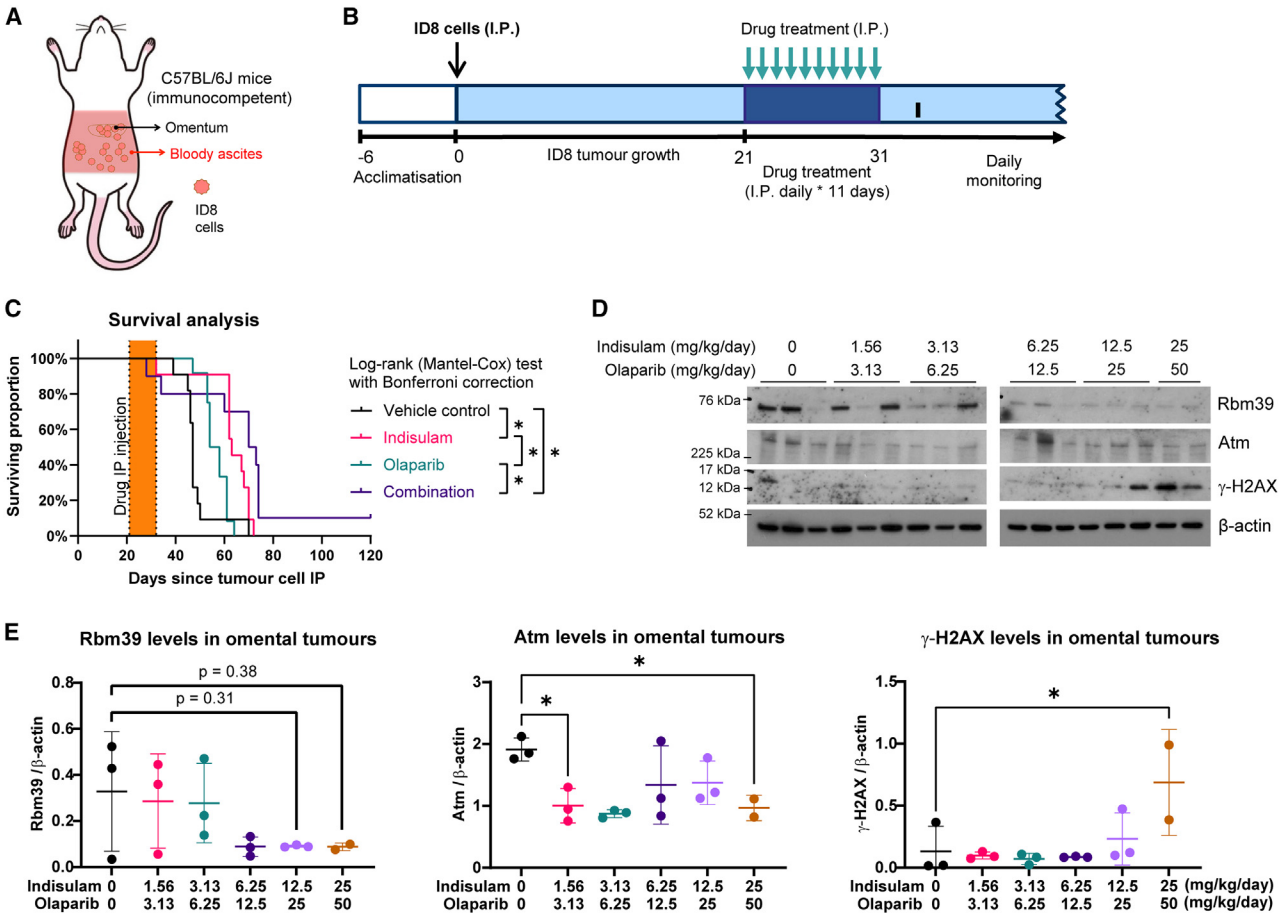

Figure 5. Indisulam improves olaparib response *in vivo*

(A and B) Schematic of ID8 murine HGSC model with the formation of peritoneal metastasis and ascites and study design.

(C) Kaplan-Meier survival curves of mice bearing ID8 tumors after indicated treatments (n = 11 for vehicle control, n = 11 for indisulam, n = 12 for olaparib, and n = 10 for drug combination). Statistical significance was calculated using the log rank (Mantel-Cox) test and Bonferroni multiple comparisons test. *p < 0.0083 (Bonferroni-corrected threshold).

(D) Western blot assessment of omental tumor samples collected from mice with indicated drug doses daily for 7 days (or 5 days in the case of the highest dose).

(E) Densitometry analysis of Rbm39, Atm, and γ-H2AX bands intensities in (d). Error bar = SD. One-way ANOVA and Dunnett's multiple comparisons test were used for statistical analysis. *p < 0.05. I.P., intraperitoneal.

that induces rapid depletion of RBM39 through DCAF15-mediated proteasomal degradation, resulting in splicing defects[32,33,35,36,103] and tumor regression in multiple animal models.[32,34–36] Indisulam and 3 other anticancer aryl sulfonamides have been tested in at least 47 clinical trials, but only 1 clinical trial involved patients with ovarian cancer (reviewed in[31]). Monotherapy of aryl sulfonamides demonstrated minor to moderate clinical benefits and most of them failed to progress beyond a phase II trial.[31] Although some tumors may be sensitive to RBM39 depletion alone (e.g., neuroblastoma[36,37]), here we demonstrate a rational case for the combination therapy of aryl sulfonamides and DNA damaging agents like platinum and PARP inhibitors in ovarian HGSC. Although DCAF15 is necessary for RBM39-mediated cytotoxicity and mRNA levels of *DCAF15* correlate with sensitivity *in vitro*, expression of *DCAF15* did not predict sensitivity to indisulam in AML patient samples.[98] This highlights the need for careful consideration for the use of DCAF15 as a clinical biomarker and the potential importance of additional biomarkers in future development. Nonetheless, the availability of drug pharmacodynamic, pharmacokinetic, and safety data in patients for both aryl sulfonamides and PARP inhibitors should aid rapid translation of such combinations to clinical studies.

In summary, this study provides strong evidence that combining RBM39 protein degraders and PARP inhibitors could be an effective therapeutic strategy for ovarian HGSC. As dosing schedules of indisulam and olaparib have been optimized in the clinic, a clinical trial could be readily designed and conducted to evaluate the safety and efficacy of such combination therapy in patients. Future studies on RBM39 function and its involvement in DNA damage repair pathways and replication stress may reveal novel biomarkers besides DCAF15 that can predict patient response to RBM39-targeted therapies. We expect that the benefit of this combination therapy could extend to other

cancers where DNA damaging agents and PARP inhibitors are approved clinically, such as breast cancer and prostate cancer.

Limitations of the study

Despite our best efforts, we were unable to confirm the loss of DCAF15 protein expression in our knockdown or knockout cells, because commercially available antibodies showed poor specificity.[104] Future analysis using a selective DCAF15 antibody would be desirable to ascertain our findings. A further caveat in our study is that the epithelial origin of ID8 cells does not represent the fallopian tube origin of most HGSC.[78,105,106] Future studies using alternative HGSC models, such as genetically engineered murine models[107] and patient-derived models,[108] would be important to validate our findings.

STAR★METHODS

Detailed methods are provided in the online version of this paper and include the following:

- KEY RESOURCES TABLE
- RESOURCE AVAILABILITY
  - Lead contact
  - Materials availability
- EXPERIMENTAL MODEL AND STUDY PARTICIPANT DETAILS
  - Cell lines and cell culture
  - CRISPR-Cas9 knockout of *DCAF15*
  - *In vivo* experiments
- METHOD DETAILS
  - Chemicals for *in vitro* use
  - Systematic literature analysis
  - RNA sequencing and data analysis
  - Functional annotation and enrichment analysis
  - PCR-based alternative splicing analysis
  - Quantitative real-time PCR
  - Protein extraction
  - Western blotting
  - Sulforhodamine B (SRB) cell growth assay
  - Drug combination and synergy analysis
  - Caspase 3/7 activation apoptosis assay
  - Annexin V cell apoptosis analysis
  - Colony formation assay
  - Cell cycle analysis
  - DNA fiber analysis
  - Immunofluorescence analysis
  - Data availability
- QUANTIFICATION AND STATISTICAL ANALYSIS

SUPPLEMENTAL INFORMATION

Supplemental information can be found online at https://doi.org/10.1016/j.celrep.2023.113307.

ACKNOWLEDGMENTS

We thank the animal technicians from the Imperial College London CBS animal center and Fabio Grundland-Freile for supporting animal studies. We thank Imperial NIHR BRC Genomics Center for conducting RNA sequencing. Supported by the Imperial College London and China Scholarship Council joint PhD studentship 201808060050 (Yu.X.); Imperial College London and China Scholarship Council joint PhD studentship 202208310101 (Y.M.); Imperial College London President's PhD Scholarship (Yi.X.); AstraZeneca/NIHR Imperial BRC Imperial College Research Fellowship (A.N.); CRUK Center PhD Studentship (M.G.); and Ovarian Cancer Action (S.S. and I.M.). This study was supported by the NIHR Imperial Biomedical Research Centre (BRC) (A.N. and H.C.K.).

AUTHOR CONTRIBUTIONS

Conceptualization: Yu.X., I.M., H.C.K., and A.N.; methodology: Yu.X., S.S., I.M., H.C.K., and A.N.; investigation: Yu.X., S.S., Y.M., M.P.L., M.G., F.M., Yi.X., C.W., M.R.S., and A.N.; visualization: Yu.X., M.P.L., and A.N.; funding acquisition: H.C.K. and A.N.; project administration: H.C.K. and A.N.; supervision: I.M., H.C.K., and A.N.; writing original draft: Yu.X., H.C.K., and A.N. All authors contributed to the review and editing of the paper.

DECLARATION OF INTERESTS

The authors declare no competing interests.

Received: April 26, 2023
Revised: September 4, 2023
Accepted: October 4, 2023

REFERENCES

1. Cancer-research-UK (2022). Ovarian Cancer Survival Statistics. https://www.cancerresearchuk.org/health-professional/cancer-statistics/statistics-by-cancer-type/ovarian-cancer/survival#heading-Three.
2. Lisio, M.-A., Fu, L., Goyeneche, A., Gao, Z.-h., and Telleria, C. (2019). High-Grade Serous Ovarian Cancer: Basic Sciences, Clinical and Therapeutic Standpoints. Int. J. Mol. Sci. *20*, 952. https://doi.org/10.3390/ijms20040952.
3. Tsibulak, I., Zeimet, A.G., and Marth, C. (2019). Hopes and failures in front-line ovarian cancer therapy. Crit. Rev. Oncol. Hematol. *143*, 14–19. https://doi.org/10.1016/j.critrevonc.2019.08.002.
4. Franzese, E., Centonze, S., Diana, A., Carlino, F., Guerrera, L.P., Di Napoli, M., De Vita, F., Pignata, S., Ciardiello, F., and Orditura, M. (2019). PARP inhibitors in ovarian cancer. Cancer Treat Rev. *73*, 1–9. https://doi.org/10.1016/j.ctrv.2018.12.002.
5. Cancer Genome Atlas Research Network; Berchuck, A., Birrer, M., Chien, J., Cramer, D.W., Dao, F., Dhir, R., DiSaia, P., Gabra, H., Glenn, P., et al. (2011). Integrated genomic analyses of ovarian carcinoma. Nature *474*, 609–615. https://doi.org/10.1038/nature10166.
6. Moschetta, M., George, A., Kaye, S.B., and Banerjee, S. (2016). BRCA somatic mutations and epigenetic BRCA modifications in serous ovarian cancer. Ann. Oncol. *27*, 1449–1455. https://doi.org/10.1093/annonc/mdw142.
7. Bryant, H.E., Schultz, N., Thomas, H.D., Parker, K.M., Flower, D., Lopez, E., Kyle, S., Meuth, M., Curtin, N.J., and Helleday, T. (2005). Specific killing of BRCA2-deficient tumours with inhibitors of poly(ADP-ribose) polymerase. Nature *434*, 913–917. https://doi.org/10.1038/nature03443.
8. Farmer, H., McCabe, N., Lord, C.J., Tutt, A.N.J., Johnson, D.A., Richardson, T.B., Santarosa, M., Dillon, K.J., Hickson, I., Knights, C., et al. (2005). Targeting the DNA repair defect in BRCA mutant cells as a therapeutic strategy. Nature *434*, 917–921. https://doi.org/10.1038/nature03445.
9. Poveda, A., Floquet, A., Ledermann, J.A., Asher, R., Penson, R.T., Oza, A.M., Korach, J., Huzarski, T., Pignata, S., Friedlander, M., et al. (2021). Olaparib tablets as maintenance therapy in patients with platinum-sensitive relapsed ovarian cancer and a BRCA1/2 mutation (SOLO2/ENGOT-Ov21): a final analysis of a double-blind, randomised, placebo-controlled, phase 3 trial. Lancet Oncol. *22*, 620–631.

10. Hao, J., Liu, Y., Zhang, T., He, J., Zhao, H., An, R., and Xue, Y. (2021). Efficacy and safety of PARP inhibitors in the treatment of advanced ovarian cancer: An updated systematic review and meta-analysis of randomized controlled trials. Crit. Rev. Oncol. Hematol. *157*, 103145. https://doi.org/10.1016/j.critrevonc.2020.103145.

11. Friedlander, M., Matulonis, U., Gourley, C., du Bois, A., Vergote, I., Rustin, G., Scott, C., Meier, W., Shapira-Frommer, R., Safra, T., et al. (2018). Long-term efficacy, tolerability and overall survival in patients with platinum-sensitive, recurrent high-grade serous ovarian cancer treated with maintenance olaparib capsules following response to chemotherapy. Br. J. Cancer *119*, 1075–1085. https://doi.org/10.1038/s41416-018-0271-y.

12. Yang, Y., Du, N., Xie, L., Jiang, J., Mo, J., Hong, J., Mao, D., Ng, D.M., and Shi, H. (2020). The efficacy and safety of the addition of poly ADP-ribose polymerase (PARP) inhibitors to therapy for ovarian cancer: a systematic review and meta-analysis. World J. Surg. Oncol. *18*, 151. https://doi.org/10.1186/s12957-020-01931-7.

13. Luo, J., Ou, S., Wei, H., Qin, X., and Jiang, Q. (2022). Comparative Efficacy and Safety of Poly (ADP-Ribose) Polymerase Inhibitors in Patients With Ovarian Cancer: A Systematic Review and Network Meta-Analysis. Front. Oncol. *12*, 815265. https://doi.org/10.3389/fonc.2022.815265.

14. Noordermeer, S.M., and van Attikum, H. (2019). PARP Inhibitor Resistance: A Tug-of-War in BRCA-Mutated Cells. Trends Cell Biol. *29*, 820–834. https://doi.org/10.1016/j.tcb.2019.07.008.

15. Tholen, J., and Galej, W.P. (2022). Structural studies of the spliceosome: Bridging the gaps. Curr. Opin. Struct. Biol. *77*, 102461. https://doi.org/10.1016/j.sbi.2022.102461.

16. Zhang, X., Yan, C., Hang, J., Finci, L.I., Lei, J., and Shi, Y. (2017). An Atomic Structure of the Human Spliceosome. Cell *169*, 918–929.e14. https://doi.org/10.1016/j.cell.2017.04.033.

17. Zhang, X., Yan, C., Zhan, X., Li, L., Lei, J., and Shi, Y. (2018). Structure of the human activated spliceosome in three conformational states. Cell Res. *28*, 307–322. https://doi.org/10.1038/cr.2018.14.

18. Stanley, R.F., and Abdel-Wahab, O. (2022). Dysregulation and therapeutic targeting of RNA splicing in cancer. Nat. Can. (Ott.) *3*, 536–546. https://doi.org/10.1038/s43018-022-00384-z.

19. Wang, E., and Aifantis, I. (2020). RNA Splicing and Cancer. Trends Cancer *6*, 631–644. https://doi.org/10.1016/j.trecan.2020.04.011.

20. Zhang, P., Zhang, P., Zhou, M., Jiang, H., Zhang, H., Shi, B., Pan, X., Gao, H., Sun, H., and Li, Z. (2013). Exon 4 deletion variant of epidermal growth factor receptor enhances invasiveness and cisplatin resistance in epithelial ovarian cancer. Carcinogenesis *34*, 2639–2646. https://doi.org/10.1093/carcin/bgt216.

21. Wang, Y., Bernhardy, A.J., Cruz, C., Krais, J.J., Nacson, J., Nicolas, E., Peri, S., van der Gulden, H., van der Heijden, I., O'Brien, S.W., et al. (2016). The BRCA1-Δ11q Alternative Splice Isoform Bypasses Germline Mutations and Promotes Therapeutic Resistance to PARP Inhibition and Cisplatin. Cancer Res. *76*, 2778–2790. https://doi.org/10.1158/0008-5472.Can-16-0186.

22. Paul, B.T., Blanchard, Z., Ridgway, M., and ElShamy, W.M. (2015). BRCA1-IRIS inactivation sensitizes ovarian tumors to cisplatin. Oncogene *34*, 3036–3052. https://doi.org/10.1038/onc.2014.237.

23. Wang, S., Wang, Z., Li, J., Qin, J., Song, J., Li, Y., Zhao, L., Zhang, X., Guo, H., Shao, C., et al. (2021). Splicing factor USP39 promotes ovarian cancer malignancy through maintaining efficient splicing of oncogenic HMGA2. Cell Death Dis. *12*, 294. https://doi.org/10.1038/s41419-021-03581-3.

24. Yao, S., Yuan, C., Shi, Y., Qi, Y., Sridha, R., Dai, M., and Cai, H. (2022). Alternative Splicing: A New Therapeutic Target for Ovarian Cancer. Technol. Cancer Res. Treat. *21*, 15330338211067911. https://doi.org/10.1177/15330338211067911.

25. Yue, C., Zhao, T., Zhang, S., Liu, Y., Zheng, G., and Zhang, Y. (2022). Comprehensive characterization of 11 prognostic alternative splicing events in ovarian cancer interacted with the immune microenvironment. Sci. Rep. *12*, 980. https://doi.org/10.1038/s41598-021-03836-1.

26. Ouyang, Y., Xia, K., Yang, X., Zhang, S., Wang, L., Ren, S., Zhou, H., Liu, Y., and Tang, F. (2021). Alternative splicing acts as an independent prognosticator in ovarian carcinoma. Sci. Rep. *11*, 10413. https://doi.org/10.1038/s41598-021-89778-0.

27. Liu, J., Lv, D., Wang, X., Wang, R., and Li, X. (2021). Systematic Profiling of Alternative Splicing Events in Ovarian Cancer. Front. Oncol. *11*, 622805. https://doi.org/10.3389/fonc.2021.622805.

28. Zhang, D., Zou, D., Deng, Y., and Yang, L. (2021). Systematic analysis of the relationship between ovarian cancer prognosis and alternative splicing. J. Ovarian Res. *14*, 120. https://doi.org/10.1186/s13048-021-00866-1.

29. Zhu, J., Chen, Z., and Yong, L. (2018). Systematic profiling of alternative splicing signature reveals prognostic predictor for ovarian cancer. Gynecol. Oncol. *148*, 368–374. https://doi.org/10.1016/j.ygyno.2017.11.028.

30. Gusev, A., Lawrenson, K., Lin, X., Lyra, P.C., Jr., Kar, S., Vavra, K.C., Segato, F., Fonseca, M.A.S., Lee, J.M., Pejovic, T., et al. (2019). A transcriptome-wide association study of high-grade serous epithelial ovarian cancer identifies new susceptibility genes and splice variants. Nat. Genet. *51*, 815–823. https://doi.org/10.1038/s41588-019-0395-x.

31. Xu, Y., Nijhuis, A., and Keun, H.C. (2022). RNA-binding motif protein 39 (RBM39): An emerging cancer target. Br. J. Pharmacol. *179*, 2795–2812. https://doi.org/10.1111/bph.15331.

32. Han, T., Goralski, M., Gaskill, N., Capota, E., Kim, J., Ting, T.C., Xie, Y., Williams, N.S., and Nijhawan, D. (2017). Anticancer sulfonamides target splicing by inducing RBM39 degradation via recruitment to DCAF15. Science *356*, eaal3755. https://doi.org/10.1126/science.aal3755.

33. Uehara, T., Minoshima, Y., Sagane, K., Sugi, N.H., Mitsuhashi, K.O., Yamamoto, N., Kamiyama, H., Takahashi, K., Kotake, Y., Uesugi, M., et al. (2017). Selective degradation of splicing factor CAPERalpha by anticancer sulfonamides. Nat. Chem. Biol. *13*, 675–680. https://doi.org/10.1038/nchembio.2363.

34. Ozawa, Y., Sugi, N.H., Nagasu, T., Owa, T., Watanabe, T., Koyanagi, N., Yoshino, H., Kitoh, K., and Yoshimatsu, K. (2001). E7070, a novel sulphonamide agent with potent antitumour activity in vitro and in vivo. Eur. J. Cancer *37*, 2275–2282.

35. Wang, E., Lu, S.X., Pastore, A., Chen, X., Imig, J., Chun-Wei Lee, S., Hockemeyer, K., Ghebrechristos, Y.E., Yoshimi, A., Inoue, D., et al. (2019). Targeting an RNA-Binding Protein Network in Acute Myeloid Leukemia. Cancer Cell *35*, 369–384.e7. https://doi.org/10.1016/j.ccell.2019.01.010.

36. Nijhuis, A., Sikka, A., Yogev, O., Herendi, L., Balcells, C., Ma, Y., Poon, E., Eckold, C., Valbuena, G.N., Xu, Y., et al. (2022). Indisulam targets RNA splicing and metabolism to serve as a therapeutic strategy for high-risk neuroblastoma. Nat. Commun. *13*, 1380. https://doi.org/10.1038/s41467-022-28907-3.

37. Singh, S., Quarni, W., Goralski, M., Wan, S., Jin, H., Van de Velde, L.A., Fang, J., Wu, Q., Abu-Zaid, A., Wang, T., et al. (2021). Targeting the spliceosome through RBM39 degradation results in exceptional responses in high-risk neuroblastoma models. Sci. Adv. *7*, eabj5405. https://doi.org/10.1126/sciadv.abj5405.

38. Gao, J., Aksoy, B.A., Dogrusoz, U., Dresdner, G., Gross, B., Sumer, S.O., Sun, Y., Jacobsen, A., Sinha, R., Larsson, E., et al. (2013). Integrative analysis of complex cancer genomics and clinical profiles using the cBioPortal. Sci. Signal. *6*, pl1. https://doi.org/10.1126/scisignal.2004088.

39. Cerami, E., Gao, J., Dogrusoz, U., Gross, B.E., Sumer, S.O., Aksoy, B.A., Jacobsen, A., Byrne, C.J., Heuer, M.L., Larsson, E., et al. (2012). The cBio Cancer Genomics Portal: An Open Platform for Exploring Multidimensional Cancer Genomics Data. Cancer Discov. *2*, 401–404. https://doi.org/10.1158/2159-8290.Cd-12-0095.

40. Basu, A., Bodycombe, N.E., Cheah, J.H., Price, E.V., Liu, K., Schaefer, G.I., Ebright, R.Y., Stewart, M.L., Ito, D., Wang, S., et al. (2013). An

interactive resource to identify cancer genetic and lineage dependencies targeted by small molecules. Cell *154*, 1151–1161. https://doi.org/10.1016/j.cell.2013.08.003.

41. Rees, M.G., Seashore-Ludlow, B., Cheah, J.H., Adams, D.J., Price, E.V., Gill, S., Javaid, S., Coletti, M.E., Jones, V.L., Bodycombe, N.E., et al. (2016). Correlating chemical sensitivity and basal gene expression reveals mechanism of action. Nat. Chem. Biol. *12*, 109–116. https://doi.org/10.1038/nchembio.1986.
42. Seashore-Ludlow, B., Rees, M.G., Cheah, J.H., Cokol, M., Price, E.V., Coletti, M.E., Jones, V., Bodycombe, N.E., Soule, C.K., Gould, J., et al. (2015). Harnessing Connectivity in a Large-Scale Small-Molecule Sensitivity DatasetHarnessing Connectivity in a Sensitivity Dataset. Cancer Discov. *5*, 1210–1223.
43. Lu, S.X., De Neef, E., Thomas, J.D., Sabio, E., Rousseau, B., Gigoux, M., Knorr, D.A., Greenbaum, B., Elhanati, Y., Hogg, S.J., et al. (2021). Pharmacologic modulation of RNA splicing enhances anti-tumor immunity. Cell *184*, 4032–4047.e31. https://doi.org/10.1016/j.cell.2021.05.038.
44. Mai, S., Qu, X., Li, P., Ma, Q., Liu, X., and Cao, C. (2016). Functional interaction between nonreceptor tyrosine kinase c-Abl and SR-Rich protein RBM39. Biochem. Biophys. Res. Commun. *473*, 355–360. https://doi.org/10.1016/j.bbrc.2016.03.108.
45. Shen, S., Park, J.W., Lu, Z.X., Lin, L., Henry, M.D., Wu, Y.N., Zhou, Q., and Xing, Y. (2014). rMATS: robust and flexible detection of differential alternative splicing from replicate RNA-Seq data. Proc. Natl. Acad. Sci. USA *111*, E5593–E5601. https://doi.org/10.1073/pnas.1419161111.
46. Choi, M., Kipps, T., and Kurzrock, R. (2016). ATM Mutations in Cancer: Therapeutic Implications. Mol. Cancer Ther. *15*, 1781–1791. https://doi.org/10.1158/1535-7163.Mct-15-0945.
47. Telatar, M., Teraoka, S., Wang, Z., Chun, H.H., Liang, T., Castellvi-Bel, S., Udar, N., Borresen-Dale, A.L., Chessa, L., Bernatowska-Matuszkiewicz, E., et al. (1998). Ataxia-telangiectasia: identification and detection of founder-effect mutations in the ATM gene in ethnic populations. Am. J. Hum. Genet. *62*, 86–97. https://doi.org/10.1086/301673.
48. Lykke-Andersen, S., and Jensen, T.H. (2015). Nonsense-mediated mRNA decay: an intricate machinery that shapes transcriptomes. Nat. Rev. Mol. Cell Biol. *16*, 665–677. https://doi.org/10.1038/nrm4063.
49. Domcke, S., Sinha, R., Levine, D.A., Sander, C., and Schultz, N. (2013). Evaluating cell lines as tumour models by comparison of genomic profiles. Nat. Commun. *4*, 2126. https://doi.org/10.1038/ncomms3126.
50. Lord, C.J., and Ashworth, A. (2017). PARP inhibitors: Synthetic lethality in the clinic. Science *355*, 1152–1158. https://doi.org/10.1126/science.aam7344.
51. Chou, T.C., and Martin, N. (2005). CompuSyn for Drug Combinations: A Computer Program for Quantitation of Synergism and Antagonism in Drug Combinations, and the Determination of IC50 and ED50 Values (ComboSyn, Inc.).
52. Murai, J., Huang, S.Y.N., Renaud, A., Zhang, Y., Ji, J., Takeda, S., Morris, J., Teicher, B., Doroshow, J.H., and Pommier, Y. (2014). Stereospecific PARP trapping by BMN 673 and comparison with olaparib and rucaparib. Mol. Cancer Ther. *13*, 433–443. https://doi.org/10.1158/1535-7163.MCT-13-0803.
53. Murai, J., Huang, S.y.N., Das, B.B., Renaud, A., Zhang, Y., Doroshow, J.H., Ji, J., Takeda, S., and Pommier, Y. (2012). Trapping of PARP1 and PARP2 by Clinical PARP Inhibitors. Cancer Res. *72*, 5588–5599. https://doi.org/10.1158/0008-5472.CAN-12-2753.
54. Hopkins, T.A., Shi, Y., Rodriguez, L.E., Solomon, L.R., Donawho, C.K., DiGiammarino, E.L., Panchal, S.C., Wilsbacher, J.L., Gao, W., Olson, A.M., et al. (2015). Mechanistic Dissection of PARP1 Trapping and the Impact on In Vivo Tolerability and Efficacy of PARP Inhibitors. Mol. Cancer Res. *13*, 1465–1477. https://doi.org/10.1158/1541-7786.MCR-15-0191-T.
55. Hopkins, T.A., Ainsworth, W.B., Ellis, P.A., Donawho, C.K., DiGiammarino, E.L., Panchal, S.C., Abraham, V.C., Algire, M.A., Shi, Y., Olson, A.M., et al. (2019). PARP1 Trapping by PARP Inhibitors Drives Cytotoxicity in Both Cancer Cells and Healthy Bone Marrow. Mol. Cancer Res. *17*, 409–419. https://doi.org/10.1158/1541-7786.MCR-18-0138.
56. Tobalina, L., Armenia, J., Irving, E., O'Connor, M.J., and Forment, J.V. (2021). A meta-analysis of reversion mutations in BRCA genes identifies signatures of DNA end-joining repair mechanisms driving therapy resistance. Ann. Oncol. *32*, 103–112. https://doi.org/10.1016/j.annonc.2020.10.470.
57. Lin, K.K., Harrell, M.I., Oza, A.M., Oaknin, A., Ray-Coquard, I., Tinker, A.V., Helman, E., Radke, M.R., Say, C., Vo, L.T., et al. (2019). BRCA Reversion Mutations in Circulating Tumor DNA Predict Primary and Acquired Resistance to the PARP Inhibitor Rucaparib in High-Grade Ovarian Carcinoma. Cancer Discov. *9*, 210–219. https://doi.org/10.1158/2159-8290.CD-18-0715.
58. Cong, K., Peng, M., Kousholt, A.N., Lee, W.T.C., Lee, S., Nayak, S., Krais, J., VanderVere-Carozza, P.S., Pawelczak, K.S., Calvo, J., et al. (2021). Replication gaps are a key determinant of PARP inhibitor synthetic lethality with BRCA deficiency. Mol. Cell *81*, 3128–3144.e7. https://doi.org/10.1016/j.molcel.2021.06.011.
59. Lloyd, R.L., Wijnhoven, P.W.G., Ramos-Montoya, A., Wilson, Z., Illuzzi, G., Falenta, K., Jones, G.N., James, N., Chabbert, C.D., Stott, J., et al. (2020). Combined PARP and ATR inhibition potentiates genome instability and cell death in ATM-deficient cancer cells. Oncogene *39*, 4869–4883. https://doi.org/10.1038/s41388-020-1328-y.
60. Wang, C., Jette, N., Moussienko, D., Bebb, D.G., and Lees-Miller, S.P. (2017). ATM-Deficient Colorectal Cancer Cells Are Sensitive to the PARP Inhibitor Olaparib. Transl. Oncol. *10*, 190–196. https://doi.org/10.1016/j.tranon.2017.01.007.
61. Jette, N.R., Radhamani, S., Arthur, G., Ye, R., Goutam, S., Bolyos, A., Petersen, L.F., Bose, P., Bebb, D.G., and Lees-Miller, S.P. (2019). Combined poly-ADP ribose polymerase and ataxia-telangiectasia mutated/Rad3-related inhibition targets ataxia-telangiectasia mutated-deficient lung cancer cells. Br. J. Cancer *121*, 600–610. https://doi.org/10.1038/s41416-019-0565-8.
62. Sun, C., Fang, Y., Labrie, M., Li, X., and Mills, G.B. (2020). Systems approach to rational combination therapy: PARP inhibitors. Biochem. Soc. Trans. *48*, 1101–1108. https://doi.org/10.1042/bst20191092.
63. Ahn, J.Y., Schwarz, J.K., Piwnica-Worms, H., and Canman, C.E. (2000). Threonine 68 phosphorylation by ataxia telangiectasia mutated is required for efficient activation of Chk2 in response to ionizing radiation. Cancer Res. *60*, 5934–5936.
64. Burma, S., Chen, B.P., Murphy, M., Kurimasa, A., and Chen, D.J. (2001). ATM phosphorylates histone H2AX in response to DNA double-strand breaks. J. Biol. Chem. *276*, 42462–42467. https://doi.org/10.1074/jbc.C100466200.
65. Stiff, T., O'Driscoll, M., Rief, N., Iwabuchi, K., Löbrich, M., and Jeggo, P.A. (2004). ATM and DNA-PK function redundantly to phosphorylate H2AX after exposure to ionizing radiation. Cancer Res. *64*, 2390–2396. https://doi.org/10.1158/0008-5472.can-03-3207.
66. Cleaver, J.E. (2011). γH2Ax: Biomarker of Damage or Functional Participant in DNA Repair "All that Glitters Is not Gold. Photochem. Photobiol. *87*, 1230–1239. https://doi.org/10.1111/j.1751-1097.2011.00995.x.
67. de Feraudy, S., Revet, I., Bezrookove, V., Feeney, L., and Cleaver, J.E. (2010). A minority of foci or pan-nuclear apoptotic staining of gamma-H2AX in the S phase after UV damage contain DNA double-strand breaks. Proc. Natl. Acad. Sci. USA *107*, 6870–6875. https://doi.org/10.1073/pnas.1002175107.
68. Burdak-Rothkamm, S., Short, S.C., Folkard, M., Rothkamm, K., and Prise, K.M. (2007). ATR-dependent radiation-induced gamma H2AX foci in bystander primary human astrocytes and glioma cells. Oncogene *26*, 993–1002. https://doi.org/10.1038/sj.onc.1209863.
69. Ward, I.M., and Chen, J. (2001). Histone H2AX is phosphorylated in an ATR-dependent manner in response to replicational stress. J. Biol. Chem. *276*, 47759–47762. https://doi.org/10.1074/jbc.C100569200.

70. Ward, I.M., Minn, K., and Chen, J. (2004). UV-induced ataxia-telangiectasia-mutated and Rad3-related (ATR) activation requires replication stress. J. Biol. Chem. *279*, 9677–9680. https://doi.org/10.1074/jbc.C300554200.

71. Ge, X.Q., and Blow, J.J. (2010). Chk1 inhibits replication factory activation but allows dormant origin firing in existing factories. J. Cell Biol. *191*, 1285–1297. https://doi.org/10.1083/jcb.201007074.

72. Petermann, E., Maya-Mendoza, A., Zachos, G., Gillespie, D.A.F., Jackson, D.A., and Caldecott, K.W. (2006). Chk1 requirement for high global rates of replication fork progression during normal vertebrate S phase. Mol. Cell Biol. *26*, 3319–3326. https://doi.org/10.1128/mcb.26.8.3319-3326.2006.

73. Smith, J., Tho, L.M., Xu, N., and Gillespie, D.A. (2010). The ATM-Chk2 and ATR-Chk1 pathways in DNA damage signaling and cancer. Adv. Cancer Res. *108*, 73–112. https://doi.org/10.1016/b978-0-12-380888-2.00003-0.

74. Toledo, L., Neelsen, K.J., and Lukas, J. (2017). Replication Catastrophe: When a Checkpoint Fails because of Exhaustion. Mol. Cell *66*, 735–749. https://doi.org/10.1016/j.molcel.2017.05.001.

75. Xiao, Z., Chen, Z., Gunasekera, A.H., Sowin, T.J., Rosenberg, S.H., Fesik, S., and Zhang, H. (2003). Chk1 Mediates S and G2 Arrests through Cdc25A Degradation in Response to DNA-damaging Agents. J. Biol. Chem. *278*, 21767–21773. https://doi.org/10.1074/jbc.M300229200.

76. Guo, C., Kumagai, A., Schlacher, K., Shevchenko, A., Shevchenko, A., and Dunphy, W.G. (2015). Interaction of Chk1 with Treslin negatively regulates the initiation of chromosomal DNA replication. Mol. Cell *57*, 492–505. https://doi.org/10.1016/j.molcel.2014.12.003.

77. Moiseeva, T., Hood, B., Schamus, S., O'Connor, M.J., Conrads, T.P., and Bakkenist, C.J. (2017). ATR kinase inhibition induces unscheduled origin firing through a Cdc7-dependent association between GINS and And-1. Nat. Commun. *8*, 1392. https://doi.org/10.1038/s41467-017-01401-x.

78. Walton, J., Blagih, J., Ennis, D., Leung, E., Dowson, S., Farquharson, M., Tookman, L.A., Orange, C., Athineos, D., Mason, S., et al. (2016). CRISPR/Cas9-Mediated Trp53 and Brca2 Knockout to Generate Improved Murine Models of Ovarian High-Grade Serous Carcinoma. Cancer Res. *76*, 6118–6129. https://doi.org/10.1158/0008-5472.Can-16-1272.

79. Walton, J.B., Farquharson, M., Mason, S., Port, J., Kruspig, B., Dowson, S., Stevenson, D., Murphy, D., Matzuk, M., Kim, J., et al. (2017). CRISPR/Cas9-derived models of ovarian high grade serous carcinoma targeting Brca1, Pten and Nf1, and correlation with platinum sensitivity. Sci. Rep. *7*, 16827. https://doi.org/10.1038/s41598-017-17119-1.

80. Torre, L.A., Trabert, B., DeSantis, C.E., Miller, K.D., Samimi, G., Runowicz, C.D., Gaudet, M.M., Jemal, A., and Siegel, R.L. (2018). Ovarian cancer statistics, 2018. CA A Cancer J. Clin. *68*, 284–296. https://doi.org/10.3322/caac.21456.

81. Stewart, C., Ralyea, C., and Lockwood, S. (2019). Ovarian Cancer: An Integrated Review. Semin. Oncol. Nurs. *35*, 151–156. https://doi.org/10.1016/j.soncn.2019.02.001.

82. Barber, E., and Matei, D. (2021). Immunotherapy in ovarian cancer: we are not there yet. Lancet Oncol. *22*, 903–905. https://doi.org/10.1016/s1470-2045(21)00303-x.

83. Sandhu, D., Antolin, A.A., Cox, A.R., and Jones, A.M. (2022). Identification of different side effects between PARP inhibitors and their polypharmacological multi-target rationale. Br. J. Clin. Pharmacol. *88*, 742–752. https://doi.org/10.1111/bcp.15015.

84. Abbate, F., Casini, A., Owa, T., Scozzafava, A., and Supuran, C.T. (2004). Carbonic anhydrase inhibitors: E7070, a sulfonamide anticancer agent, potently inhibits cytosolic isozymes I and II, and transmembrane, tumor-associated isozyme IX. Bioorg. Med. Chem. Lett. *14*, 217–223.

85. Supuran, C.T. (2018). Carbonic anhydrase inhibitors as emerging agents for the treatment and imaging of hypoxic tumors. Expet Opin. Invest. Drugs *27*, 963–970. https://doi.org/10.1080/13543784.2018.1548608.

86. Del Prete, S., Angeli, A., Ghobril, C., Hitce, J., Clavaud, C., Marat, X., Supuran, C.T., and Capasso, C. (2020). Sulfonamide Inhibition Profile of the β-Carbonic Anhydrase from Malassezia restricta, An Opportunistic Pathogen Triggering Scalp Conditions. Metabolites *10*, 39. https://doi.org/10.3390/metabo10010039.

87. DeWeirdt, P.C., Sangree, A.K., Hanna, R.E., Sanson, K.R., Hegde, M., Strand, C., Persky, N.S., and Doench, J.G. (2020). Genetic screens in isogenic mammalian cell lines without single cell cloning. Nat. Commun. *11*, 752. https://doi.org/10.1038/s41467-020-14620-6.

88. Tsujino, T., Takai, T., Hinohara, K., Gui, F., Tsutsumi, T., Bai, X., Miao, C., Feng, C., Gui, B., Sztupinszki, Z., et al. (2023). CRISPR screens reveal genetic determinants of PARP inhibitor sensitivity and resistance in prostate cancer. Nat. Commun. *14*, 252. https://doi.org/10.1038/s41467-023-35880-y.

89. Su, D., Feng, X., Colic, M., Wang, Y., Zhang, C., Wang, C., Tang, M., Hart, T., and Chen, J. (2020). CRISPR/CAS9-based DNA damage response screens reveal gene-drug interactions. DNA Repair *87*, 102803. https://doi.org/10.1016/j.dnarep.2020.102803.

90. Noordermeer, S.M., Adam, S., Setiaputra, D., Barazas, M., Pettitt, S.J., Ling, A.K., Olivieri, M., Álvarez-Quilón, A., Moatti, N., Zimmermann, M., et al. (2018). The shieldin complex mediates 53BP1-dependent DNA repair. Nature *560*, 117–121. https://doi.org/10.1038/s41586-018-0340-7.

91. Zimmermann, M., Murina, O., Reijns, M.A.M., Agathanggelou, A., Challis, R., Tarnauskaitė, Ž., Muir, M., Fluteau, A., Aregger, M., McEwan, A., et al. (2018). CRISPR screens identify genomic ribonucleotides as a source of PARP-trapping lesions. Nature *559*, 285–289. https://doi.org/10.1038/s41586-018-0291-z.

92. Hong, R., Ma, F., Zhang, W., Yu, X., Li, Q., Luo, Y., Zhu, C., Jiang, W., and Xu, B. (2016). 53BP1 depletion causes PARP inhibitor resistance in ATM-deficient breast cancer cells. BMC Cancer *16*, 725. https://doi.org/10.1186/s12885-016-2754-7.

93. Riches, L.C., Trinidad, A.G., Hughes, G., Jones, G.N., Hughes, A.M., Thomason, A.G., Gavine, P., Cui, A., Ling, S., Stott, J., et al. (2020). Pharmacology of the ATM Inhibitor AZD0156: Potentiation of Irradiation and Olaparib Responses Preclinically. Mol. Cancer Ther. *19*, 13–25. https://doi.org/10.1158/1535-7163.Mct-18-1394.

94. Brill, E., Yokoyama, T., Nair, J., Yu, M., Ahn, Y.R., and Lee, J.M. (2017). Prexasertib, a cell cycle checkpoint kinases 1 and 2 inhibitor, increases in vitro toxicity of PARP inhibition by preventing Rad51 foci formation in BRCA wild type high-grade serous ovarian cancer. Oncotarget *8*, 111026–111040. https://doi.org/10.18632/oncotarget.22195.

95. Smith, H.L., Prendergast, L., and Curtin, N.J. (2020). Exploring the Synergy between PARP and CHK1 Inhibition in Matched BRCA2 Mutant and Corrected Cells. Cancers *12*, 878. https://doi.org/10.3390/cancers12040878.

96. Anderson, V.E., Walton, M.I., Eve, P.D., Boxall, K.J., Antoni, L., Caldwell, J.J., Aherne, W., Pearl, L.H., Oliver, A.W., Collins, I., and Garrett, M.D. (2011). CCT241533 is a potent and selective inhibitor of CHK2 that potentiates the cytotoxicity of PARP inhibitors. Cancer Res. *71*, 463–472. https://doi.org/10.1158/0008-5472.CAN-10-1252.

97. Matveeva, E., Maiorano, J., Zhang, Q., Eteleeb, A.M., Convertini, P., Chen, J., Infantino, V., Stamm, S., Wang, J., Rouchka, E.C., and Fondufe-Mittendorf, Y.N. (2016). Involvement of PARP1 in the regulation of alternative splicing. Cell Discov. *2*, 15046. https://doi.org/10.1038/celldisc.2015.46.

98. Matveeva, E.A., Al-Tinawi, Q.M.H., Rouchka, E.C., and Fondufe-Mittendorf, Y.N. (2019). Coupling of PARP1-mediated chromatin structural changes to transcriptional RNA polymerase II elongation and cotranscriptional splicing. Epigenet. Chromatin *12*, 15. https://doi.org/10.1186/s13072-019-0261-1.

99. Matveeva, E.A., Mathbout, L.F., and Fondufe-Mittendorf, Y.N. (2019). PARP1 is a versatile factor in the regulation of mRNA stability and decay. Sci. Rep. *9*, 3722. https://doi.org/10.1038/s41598-019-39969-7.

100. Ke, J., Liu, F., Tu, Y., Cai, Z., Luo, Y., and Wu, X. (2021). PARP1–RNA interaction analysis: PARP1 regulates the expression of extracellular matrix-related genes in HK-2 renal proximal tubular epithelial cells. FEBS Lett. *595*, 1375–1387. https://doi.org/10.1002/1873-3468.14065.

101. Loerch, S., Maucuer, A., Manceau, V., Green, M.R., and Kielkopf, C.L. (2014). Cancer-relevant splicing factor CAPERalpha engages the essential splicing factor SF3b155 in a specific ternary complex. J. Biol. Chem. *289*, 17325–17337. https://doi.org/10.1074/jbc.M114.558825.

102. Owa, T., Yoshino, H., Okauchi, T., Yoshimatsu, K., Ozawa, Y., Sugi, N.H., Nagasu, T., Koyanagi, N., and Kitoh, K. (1999). Discovery of novel antitumor sulfonamides targeting G1 phase of the cell cycle. J. Med. Chem. *42*, 3789–3799.

103. Ting, T.C., Goralski, M., Klein, K., Wang, B., Kim, J., Xie, Y., and Nijhawan, D. (2019). Aryl Sulfonamides Degrade RBM39 and RBM23 by Recruitment to CRL4-DCAF15. Cell Rep. *29*, 1499–1510.e6. https://doi.org/10.1016/j.celrep.2019.09.079.

104. Hsiehchen, D., Goralski, M., Kim, J., Xie, Y., and Nijhawan, D. (2020). Biomarkers for RBM39 degradation in acute myeloid leukemia. Leukemia *34*, 1924–1928. https://doi.org/10.1038/s41375-020-0729-9.

105. Lee, Y., Miron, A., Drapkin, R., Nucci, M.R., Medeiros, F., Saleemuddin, A., Garber, J., Birch, C., Mou, H., Gordon, R.W., et al. (2007). A candidate precursor to serous carcinoma that originates in the distal fallopian tube. J. Pathol. *211*, 26–35. https://doi.org/10.1002/path.2091.

106. Salvador, S., Gilks, B., Köbel, M., Huntsman, D., Rosen, B., and Miller, D. (2009). The fallopian tube: primary site of most pelvic high-grade serous carcinomas. Int. J. Gynecol. Cancer *19*, 58–64. https://doi.org/10.1111/IGC.0b013e318199009c.

107. Maniati, E., Berlato, C., Gopinathan, G., Heath, O., Kotantaki, P., Lakhani, A., McDermott, J., Pegrum, C., Delaine-Smith, R.M., Pearce, O.M.T., et al. (2020). Mouse Ovarian Cancer Models Recapitulate the Human Tumor Microenvironment and Patient Response to Treatment. Cell Rep. *30*, 525–540.e7. https://doi.org/10.1016/j.celrep.2019.12.034.

108. Coulson-Gilmer, C., Morgan, R.D., Nelson, L., Barnes, B.M., Tighe, A., Wardenaar, R., Spierings, D.C.J., Schlecht, H., Burghel, G.J., Foijer, F., et al. (2021). Replication catastrophe is responsible for intrinsic PAR glycohydrolase inhibitor-sensitivity in patient-derived ovarian cancer models. J. Exp. Clin. Cancer Res. *40*, 323. https://doi.org/10.1186/s13046-021-02124-0.

109. Dobin, A., Davis, C.A., Schlesinger, F., Drenkow, J., Zaleski, C., Jha, S., Batut, P., Chaisson, M., and Gingeras, T.R. (2013). STAR: ultrafast universal RNA-seq aligner. Bioinformatics *29*, 15–21. https://doi.org/10.1093/bioinformatics/bts635.

110. Schindelin, J., Arganda-Carreras, I., Frise, E., Kaynig, V., Longair, M., Pietzsch, T., Preibisch, S., Rueden, C., Saalfeld, S., Schmid, B., et al. (2012). Fiji: an open-source platform for biological-image analysis. Nat. Methods *9*, 676–682. https://doi.org/10.1038/nmeth.2019.

111. Mai, S., Qu, X., Li, P., Ma, Q., Cao, C., and Liu, X. (2016). Global regulation of alternative RNA splicing by the SR-rich protein RBM39. Biochim. Biophys. Acta *1859*, 1014–1024. https://doi.org/10.1016/j.bbagrm.2016.06.007.

112. Huang, D.W., Sherman, B.T., and Lempicki, R.A. (2009). Systematic and integrative analysis of large gene lists using DAVID bioinformatics resources. Nat. Protoc. *4*, 44–57. https://doi.org/10.1038/nprot.2008.211.

113. Sherman, B.T., Hao, M., Qiu, J., Jiao, X., Baseler, M.W., Lane, H.C., Imamichi, T., and Chang, W. (2022). DAVID: a web server for functional enrichment analysis and functional annotation of gene lists (2021 update). Nucleic Acids Res. *50*, W216–W221. https://doi.org/10.1093/nar/gkac194.

114. Schmittgen, T.D., and Livak, K.J. (2008). Analyzing real-time PCR data by the comparative C(T) method. Nat. Protoc. *3*, 1101–1108. https://doi.org/10.1038/nprot.2008.73.

115. Chou, T.C. (2010). Drug combination studies and their synergy quantification using the Chou-Talalay method. Cancer Res. *70*, 440–446. https://doi.org/10.1158/0008-5472.Can-09-1947.

116. Chou, T.C. (2006). Theoretical basis, experimental design, and computerized simulation of synergism and antagonism in drug combination studies. Pharmacol. Rev. *58*, 621–681. https://doi.org/10.1124/pr.58.3.10.

STAR★METHODS

KEY RESOURCES TABLE

REAGENT or RESOURCE	SOURCE	IDENTIFIER
Antibodies		
Rabbit anti-RBM39	Sigma-Aldrich	Cat# HPA001591; RRID:AB_1079749
Mouse anti-β-actin	Abcam	Cat# ab6276; RRID:AB_2223210
Mouse anti-phospho-Histone H2A.X (ser139) γH2AX	Sigma-Aldrich	Cat# 05–636; RRID:AB_309864
Rabbit anti-human pChk2 (T68)	R&D system	Cat# AF1626; RRID:AB_2291844
Rabbit anti-human Chk2	R&D system	Cat# MAB1358; RRID:AB_2941307
Rabbit anti-pATM-S1981	Abcam	Cat# ab81292; RRID:AB_1640207
Mouse anti-ATM	GenTex	Cat# GTX70103; RRID:AB_368161
Rabbit anti-pChk1-S345	Cell Signaling Technology	Cat# 2348; RRID:AB_331212
Mouse anti-Chk1	Cell Signaling Technology	Cat# 2360; RRID:AB_2080320
Mouse-*anti*-BrdU	BD Biosciences	Cat# BD347580; RRID:AB_10015219
Rat anti-BrdU	Abcam	Cat# ab6326; RRID:AB_305426
HRP-conjugated goat anti-rabbit polyclonal	Invitrogen	Cat# 31460; RRID:AB_228341
HRP-conjugated goat anti-mouse polyclonal	Invitrogen	Cat# 31340; RRID:AB_228339
AF488-conjugated goat anti-mouse	Invitrogen	Cat# A11001; RRID:AB_2534069
AF647-conjugated goat anti-rat	Invitrogen	Cat# A21247; RRID:AB_141778
Bacterial and virus strains		
Edit-R CRISPR-Cas9-TurboGFP lentiviral particles	Dharmacon	Cat# VCAS11864
Chemicals, peptides, and recombinant proteins		
Indisulam	Sigma-Aldrich	Cat# SML1225
E7820	Sigma-Aldrich	Cat# SML2950
Olaparib	Selleckchem	Cat# S1060
Rucaparib phosphate	Selleckchem	Cat# S1098
Veliparib	Selleckchem	Cat# S1004
Niraparib	Selleckchem	Cat# S2741
IdU	Sigma-Aldrich	Cat# I7125
BrdU	Sigma-Aldrich	Cat# B5002
Z-VAD-FMK	APExBIO	Cat# A1902
Agarose	Sigma-Aldrich	Cat# A9539
HALT protease and phosphatase inhibitor cocktail	Thermo Scientific	Cat# 78442
Sulforhodamine B	Sigma-Aldrich	Cat# S1402
Cy5.5-conjugated Annexin V	BD Biosciences	Cat# 559925
Propidium Iodide staining solution	Invitrogen	Cat# 00-6990-50
Formaldehyde, Methanol-free	Thermo Scientific	Cat# 11586711
Triton X-100	Sigma-Aldrich	Cat# T8787
DAPI	Sigma-Aldrich	Cat# D9542
Critical commercial assays		
miRNeasy Mini Kit	Qiagen	Cat# 217084
RNeasy Mini Kit	Qiagen	Cat# 74106
High-Capacity RNA-to-cDNA kit	Applied Biosystems	Cat# 4387406
Q5 High-Fidelity PCR kit	New England Biolabs	Cat# E0555
Restore WB stripping buffer	Thermo Scientific	Cat# 21059

(*Continued on next page*)

Continued

REAGENT or RESOURCE	SOURCE	IDENTIFIER
Caspase-Glo 3/7 Assay System	Promega	Cat# G8093
Deposited data		
RNA sequencing data	This paper	Data available through the NCBI GEO Series accession number GSE223011
Experimental models: Cell lines		
KURAMOCHI cell line	Gift from Dr Haonan Lu (Imperial College London)	N/A
OVSAHO cell line	Japanese Collection of Research Bioresources (JCRB)	RRID:CVCL_3114
OVISE cell line	JCRB	RRID:CVCL_3116
COV318 cell line	European Collection of Authenticated Cell Culture (ECACC)	Cat# 07071903; RRID:CVCL_2419
COV504 cell line	ECACC	Cat# 07071902; RRID:CVCL_2424
COV644 cell line	ECACC	Cat# 07071908; RRID:CVCL_2425
PEO1 parental cell line for CRISPR editing	Gift from Professor Bob Brown lab (Imperial College London)	N/A
PEO1	Public Health England	Cat# 10032308; RRID:CVCL_2686
PEO4	Public Health England	Cat# 10032309; RRID:CVCL_2690
ID8-*Trp53*$^{-/-}$ murine cell line	Gift from Professor I. McNeish lab (Imperial College London)	N/A
ID8-*Trp53*$^{-/-}$;*Brca2*$^{-/-}$murine cell line	Gift from Professor I. McNeish lab (Imperial College London)	N/A
Experimental models: Organisms/strains		
Mouse (female)	Charles River Laboratory (UK)	C57BL/6J
Oligonucleotides		
Edit-R CRISPR-Cas9 synthetic tracrRNA	Horizon	U-002005
Edit-R crRNA Non-Targeting Control	Horizon	U-007501-01
Edit-R crRNA custom sequence (DCAF15)	Horizon	N/A
DCAF15 TaqMan gene expression probe	Thermo Scientific	Hs00384913_m1
BACT TaqMan gene expression probe	Thermo Scientific	Hs01060665_g1
Software and algorithms		
STAR (Spliced Transcripts Alignment to a Reference) (v2.5.2b)	(Dobin et al.)[109]	https://github.com/alexdobin/STAR
SpliceFisher	GitHub	https://github.com/jiwoongbio/SpliceFisher
rMATS	(Shen et al.)[45]	https://rnaseq-mats.sourceforge.io/
The Database for Annotation, Visualization and Integrated Discovery (DAVID)	Laboratory of Human Retrovirology and Immunoinformatics	https://david.ncifcrf.gov/summary.jsp
Integrative Genomics Viewer (version 2.15.2)	Broad Institute	https://software.broadinstitute.org/software/igv/
GRCh38 human reference genome	Ensembl	https://useast.ensembl.org/Homo_sapiens/Info/Index
Annealing temperature calculator	New England Biolabs	https://tmcalculator.neb.com/#!/main
ImageJ Fiji V2.0.0	(Schindelin et al.)[110]	https://imagej.net/software/fiji/
CompuSyn	(Chou et al.)[51]	https://www.combosyn.com
Prism 9	GraphPad	https://www.graphpad.com/features
CellProfiler (V3.1.8.)	Broad Institute	https://cellprofiler.org
Other		
Lipofectamine 2000	Life Technologies	Cat# 11668019
SYBR™ Safe DNA Gel Stain	Invitrogen	Cat# S33102
Mini-PROTEAN precast gels	Bio-Rad	Cat# 4561033
Supersignal West Pico PLUS chemiluminescent substrate	Thermo Scientific	Cat# 34580
Amersham Hyperfilm ECL	Cytiva Life Sciences	Cat# 28906839
Fluoromount-G	Invitrogen	Cat# 00-4958-02

RESOURCE AVAILABILITY

Lead contact

Further information and requests for resources and reagents should be directed to and will be fulfilled by the lead contact, Anke Nijhuis (a.nijhuis@imperial.ac.uk).

Materials availability

All materials generated in this study are available upon request.

Data and code availability

RNA-seq data have been deposited at GEO under the accession number GEO:GSE223011 and are publicly available as of the date of publication. This paper does not report original codes. Any additional information required to reanalyze the data reported in this work paper is available from the lead contact upon request.

EXPERIMENTAL MODEL AND STUDY PARTICIPANT DETAILS

Cell lines and cell culture

KURAMOCHI was acquired from Dr. Haonan Lu, Imperial College London. OVSAHO and OVISE were purchased from the Japanese Collection of Research Bioresources (JCRB) cell bank. COV318, COV504, and COV644 were obtained from the European Collection of Authenticated Cell Culture (ECACC). The PEO1 cells for *DCAF15* knockdown or knockout experiments had a missense reversion mutation 5192A>T in *BRCA2*, and it was a kind gift from Professor Bob Brown's laboratory, Imperial College London. An independent stock of PEO1 (without the reversion mutation) was purchased from the Public Health England and used for dose-response curves and synergy analysis without CRISPR-Cas9 editing. PEO4 was purchased from Public Health England. Mouse ovarian cancer cell line ID8-*Trp53*$^{-/-}$ and ID8-*Trp53*$^{-/-}$;*Brca2*$^{-/-}$ lines were directly obtained from Professor Iain McNeish's laboratory.[78] All cell lines were tested regularly for mycoplasma contamination and authenticated in 2018–2019 (case #11232) and 2023 (Case #.

OVSAHO and OVISE cells were cultured in RPMI-1640 media (Gibco) supplemented with 10% fetal bovine serum (FBS, Gibco, or FirstLink), 2 mM of L-glutamine (Gibco), and 100 units/mL of penicillin-streptomycin (Gibco). PEO1-derived cells and PEO4 were cultured in RPMI-1640 supplemented with 10% FBS, 2 mM L-glutamine, 100 units/mL of penicillin-streptomycin, and 2 mM sodium pyruvate (Gibco). COV318, COV504, COV644, and KURAMOCHI cells were cultured in DMEM media (Gibco, without glucose or phenol red) supplemented with 10% FBS, 2 mM L-glutamine, 100 units/mL of penicillin-streptomycin, and 5.6 mM glucose (Gibco). ID8 clones were cultured in DMEM media (without glucose or phenol red) supplemented with 4% FBS, 2 mM L-glutamine, 100 units/mL of penicillin-streptomycin, 25 mM glucose, and 1x Insulin-Transferrin-Selenium solution (Gibco).[78] All cells were cultured at 37°C with 5% CO_2.

CRISPR-Cas9 knockout of *DCAF15*

PEO1 cells were seeded in 96-well plates and transduced with Edit-R CRISPR-Cas9-TurboGFP lentiviral particles (Dharmacon #VCAS11864). Transduced cells with GFP expression were sorted via FACS. PEO1-Cas9 cells were then expanded and transfected with 50nM *DCAF15* targeting crRNA (5′-GCAGCTTCCGGAAGAGGCGA-3′)[32] and 50nM Edit-R CRISPR-Cas9 synthetic tracrRNA (Dharmacon #U-002005) using lipofectamine 2000 (Life Technologies). Edit-R crRNA Non-Targeting Control (Dharmacon #U-007501-01) was used alongside as a negative control. Following transfection, single-cell clones were expanded and sequenced for *DCAF15* editing. Loss of DCAF15 function was validated using indisulam dose response studies. Disruption of genomic *DCAF15* was confirmed by DNA sequencing (Figure S12). Unfortunately, DCAF15 expression at protein levels were not confirmed by Western blot due to a lack of DCAF15-specific antibodies[104,104].

In vivo experiments

Animal studies were designed and conducted in accordance with the UK Animals (Scientific Procedures) Act 1986. Mice were kept at the Central Biomedical Services (CBS), Imperial College London. All individuals involved were Home Office Personal License holders working under the Project License (PA780D61A). C57BL/6J female mice aged between 6 and 7 weeks were purchased from the Charles River Laboratory (UK). Newly arrived mice were acclimatized for seven days before regulated procedures. Then, five million ID8-*Trp53*$^{-/-}$ cells were injected intraperitoneally (I.P.) into each mouse and allowed to proliferate for at least 21 days before drug treatments.

Drug solutions of vehicle control (3.5% DMSO and 6.5% Tween-80 in saline) indisulam (Sigma-Aldrich, #SML1225), or olaparib (Selleckchem, #S1060) were prepared for *in vivo* administration.[32,34,36] Left and right abdomen were alternated for I.P. injections (11 days) to minimize animal discomfort. For pharmacodynamic experiments, mice were randomly enrolled into 4 treatment groups (n = 3 mice per group) and were culled within 48 h after the last dosing. For survival studies, mice (n = 11 for vehicle control, n = 11 for indisulam, n = 12 for olaparib, and n = 10 for drug combination) were monitored until end of study (day 120) or when humane endpoint (as per project license) was reached. At endpoint, omental tumor deposits were collected and snap-frozen in liquid nitrogen and stored at −80°C until further analysis. Five mice survived to day 120. In four of the five mice, we could not guarantee successful tumor

implantation (such as developing subcutaneous tumor deposits after injection of ID8 cells) and were excluded from the Kaplan-Meier survival analysis.

METHOD DETAILS

Chemicals for *in vitro* use

Indisulam (SML1225) and E7820 (SML2950) were purchased from Sigma-Aldrich and dissolved in dimethyl sulfoxide (DMSO) for *in vitro* use. Olaparib (S1060), rucaparib phosphate (S1098), veliparib (S1004), and niraparib (S2741) were supplied by Selleckchem and reconstituted in DMSO for *in vitro* use. The IdU (I7125) and BrdU (B5002) were purchased from Sigma-Aldrich and dissolved in 1M NH_4OH and DMSO, respectively. Z-VAD-FMK (APExBIO, #A1902) was dissolved in DMSO. All drugs were prepared and stored according to manufacturers' instructions.

Systematic literature analysis

A PubMed search using the keyword "RBM39" was performed on 10 August 2022. Inclusion criteria were defined as research articles conducted RNA sequencing in RBM39-depleted human cancer cell lines, and the list of alternatively spliced genes is publicly available. Exclusion criteria were non-research articles, non-human cancer cell lines, and non-publicly available alternative splicing data. After full-text reading, five articles containing 11 lists of alternatively spliced genes were included for analysis[35–37,43,111].[35-37,43,111] Exon-skipped genes and intron-retained genes were extracted from each list. The occurrence of unique genes (exon-skipped or intron-retained) in was counted across 11 lists. The common splicing targets of RBM39 were defined as exon-skipped genes occurred at least six times, or intron-retained genes occurred at least six times. Duplicates were removed for enrichment analysis.

RNA sequencing and data analysis

KURAMOCHI cells were treated with 0.1% DMSO or 10 μM indisulam for 24 h. The total RNA was extracted using the miRNeasy Mini Kit (Qiagen, #217084) following manufacturer's protocol. RNA samples of three biological repeats were sent for sequencing at the National Institute for Health and Care Research-funded Imperial Biomedical Research Center (BRC) Genomics Facility. All samples passed Quality Control assessment using a Tapestation. Samples were sequenced using a Nextseq2000 P2 (200 cycles) sequencer, and 100 bp paired-end reads were generated. Quality control checks were performed using FastQC. The GRCh38 reference genome (unmasked primary assembly) and GTF file (release 107) were downloaded from Ensembl (http://www.ensembl.org/info/data/ftp/index.html). STAR was used to align reads to the reference genome and read counts per gene were determined using featureCounts 109. The alternative splicing analysis was performed SpliceFisher[32] and rMATS algorithms.[45] Sashimi plots were generated using Integrative Genomics Viewer (IGV, version 2.15.2, Broad Institute). Exon annotations were based on the GRCh38 human reference genome (http://uswest.ensembl.org/index.html). RNAseq data has been uploaded to the NCBI Gene Expression Omnibus and are accessible through GEO Series accession number GSE223011.

Functional annotation and enrichment analysis

The Database for Annotation, Visualization and Integrated Discovery (DAVID, https://david.ncifcrf.gov/summary.jsp)[112,113] was used for functional annotation and enrichment analysis with four databases selected: Gene ontology biological processes (DIRECT), Kyoto Encyclopedia of Genes and Genomes (KEGG), REACTOME, and WIKIPATHWAY. A query-specific background gene list was used whenever possible. Significant enrichment was defined as terms or pathways with FDR less than 0.1.

PCR-based alternative splicing analysis

Total RNA from cells was extracted using the RNeasy Mini Kit (Qiagen, #74106) or miRNeasy Mini Kit (Qiagen, #217084) following the supplier's instructions with on-column DNase digestion. Equal quantities of RNA were reverse transcribed to cDNA using the High-Capacity RNA-to-cDNA kit (Applied Biosystems). To detect alternative splicing variants, we designed primers flanking the regions of interest (sequence provided below) and amplified them using the Q5 High-Fidelity PCR kit (New England Biolabs). PCR reactions included 35 cycles, and annealing temperatures were calculated using the annealing temperature calculator (https://tmcalculator.neb.com/#!/main). PCR products were electrophoresed using 2–3% agarose (Sigma-Aldrich) gels mixed with 1:10,000 SYBRsafe DNA gel stain (Invitrogen). Gels were visualized with a GelDoc.

Primers used in this study included *ATM* (exon 51 to 54) forward 5′- TGCCTCTTATGTACCAATTGGCT-3′, reverse 5′-AATTGGCTGGTCTGCTGGAA-3'; *BRCA1* (exon 7 to 10) forward 5′-AACTCTGAGGACAAAGCAGC-3′, reverse 5′-CTGTAATGAGCTGGCATGAGT-3'; *RAD51D* (exon 3 to 6) forward 5′-TGGCTCAGTTCTCGGCTTT-3′, reverse 5′- AGATGTCAAATGCATGCACCA-3'; *TP53BP1* (exon 15 to 18) forward 5′- GCTGTTGCTGAGTCTGTTGC-3′, reverse 5′-TGCGTACTTCCCGGATTGTT-3'; *RIF1* (exon 21 to 23) forward 5′-AGGTGGGCAAAACTGGTCAT -3′, reverse 5′-TGGGTGCTCCACTACGAAAT-3'; *FANCI* (exon 31 to 35) forward 5′- GAGTCAGGCCGAGAAGGTTC-3′, reverse 5′- CAACGGCAGCAGGTTTCTC-3'; and *GAPDH* forward 5′-GGCTGCTTTTAACTCTGG-3′, reverse 5′-GGAGGGATCTCGCTCC-3'.

Quantitative real-time PCR

Total RNA from cell lines was extracted directly from culture flasks using the RNeasy Mini Kit (Qiagen, #74106) following the supplier's instructions. Equal quantities of RNA were reverse transcribed to cDNA using the High-Capacity RNA-to-cDNA kit (Applied Biosystems). *DCAF15* gene expression was measured using TaqMan gene expression probes (Hs00384913_m1) normalized to BACT (Hs01060665_g1) according to manufacturer's guidelines (ThermoFisher). Analysis was conducted using the comparative CT method.[114]

Protein extraction

Total proteins of cultured cells were extracted using RIPA lysis buffer (Sigma-Aldrich, #R0278) supplemented with at least 1% HALT protease and phosphatase inhibitor cocktail (ThermoFisher, #78442). Proteins from tumor tissues were extracted in RIPA buffer supplemented with 3% protease and phosphatase inhibitor cocktail at a rate of 50-100μL lysis buffer per 10 mg tissue. To facilitate protein extraction, tissues were mixed with glass grinding beads and homogenized by the Cryolys Evolution homogenizer, followed by sonication in an ice bath for 10–20 min. Protein supernatants were collected after centrifugation at 20,000xg at 4°C for 20 min and stored at −80°C until analysis.

Western blotting

An equal amount of protein was loaded onto triglycine Mini-PROTEAN precast gels (Bio-Rad) for electrophoresis (200V for 35 to 50 min), followed by wet transfer (100V for 60 min) to nitrocellulose membrane via wet transfer. Membranes were blocked in 5% skimmed milk in tris-buffered saline containing 0.1% of Tween 20 (TBST) or 5% bovine serum albumin (in TBST, for phosphorylated targets) for 60 min at room temperature. Primary antibodies were diluted in 5% skimmed milk and incubated overnight at 4°C. Horseradish peroxidase (HRP)-conjugated secondary antibodies were diluted in 5% skimmed milk and incubated for 60 min at room temperature. Before and after each antibody incubation, membranes were washed three times with TBST. Proteins of interest were detected with the SuperSignal West Pico PLUS chemiluminescent substrate (Thermo Scientific) and Amersham Hyperfilm ECL (GE Healthcare). ImageJ Fiji V2.0.0 was used for protein bands densitometry analysis. Membranes might be stripped once with the Restore WB stripping buffer (Thermo Scientific, #21059) and re-probed with a different pair of primary and secondary antibodies.

Primary antibodies used in this studies were rabbit anti-RBM39 (1:500, Sigma-Aldrich, #HPA001591), mouse-*anti*-β-actin (1:10,000 - 1:50,000, Abcam, #ab6276), mouse anti-phospho-Histone H2A.X (ser139) γH2AX (1:1000, Sigma-Aldrich, #05–636), rabbit anti-human pChk2 (T68) (1:300, R&D system, AF1626), rabbit anti-human Chk2 (1:500, R&D system, MAB1358), rabbit anti-pATM-S1981 (1:2000, Abcam, #ab81292), mouse anti-ATM (1:1000, GenTex, GTX70103), rabbit anti-pChk1-S345 (Cell Signaling Technology, CST2348, 1:1000), and mouse anti-Chk1 (Cell Signaling Technology, CST2360). HRP-conjugated secondary antibodies included goat anti-rabbit polyclonal antibody (1:2500 - 1:5000, Invitrogen, #31460), and goat anti-mouse polyclonal antibody (1:2500–1:5000, Invitrogen, #31340).

Sulforhodamine B (SRB) cell growth assay

SRB dye was supplied by Sigma-Aldrich. For a 48 or 72-h growth assay, cells were counted using a hemocytometer (Hawksley) and seeded in 96-well plates at the following densities: 500 cells per well (ID8 cells), 2000 cells per well (OVISE, COV318, and COV504), 2500 cells per well (PEO1-derived cells), 4000 cells per well (PEO4, COV644, and KURAMOCHI), and 5000 per well (OVSAHO). Cells were allowed to attach overnight before drug treatment the next day. At the end of drug treatment, cells were fixed with 10% (w/v) of trichloroacetic acid (TCA) solution at 4°C for 60 min and rinsed gently under tap water. Plates were left on the bench to dry before staining with 0.4% SRB solution (in 1% acetic acid) for 30 min. Excess SRB dye was washed away with 1% acetic acid. After drying on the bench, 10 mM Tris-base was added to each well to solubilize the protein-bound dye. Cell growth was measured using absorbance at 565 nm or 510 nm with a plate reader (OPTImax Molecular Devices or BMG Labtech ClarioStar). A blank control without cells was included for background subtraction. Cell growth values under drug treatment were normalized to vehicle control (0.1%–0.2% DMSO).

Drug combination and synergy analysis

Drug-drug interactions were assessed using the Chou-Talalay method[51,115,116] A fixed combination ratio for each drug pairs was experimentally determined by concentrations that caused similar cytotoxicity (30%–50% growth inhibition). CI values were calculated using the CompuSyn.[51] CI < 1 indicates synergism, CI = 1 indicates additive, and CI > 1 indicates antagonism.

Caspase 3/7 activation apoptosis assay

Cells were seeded and treated in the same way as SRB assays. After 48-h treatment, the conditioned media was aspirated and replaced with 30–50 μL of fresh media. An equal volume of the Caspase-Glo 3/7 reagent (Promega, G8093) was added and incubated on a shaker for at least 45 min. The reaction mixture from each well was then transferred to an opaque-walled 96-well plate for measurement by a ClarioStar plate reader (BMG Labtech). A cell-free control was involved for background correction. A parallel plate was always included to quantify cell mass by SRB assay, which was used to normalize caspase 3/7 levels.

Annexin V cell apoptosis analysis

After drug treatment, adhering cells were detached from plates by trypsinization (TrypLE Express, Gibco, #12604013) and combined with floating cells from the conditioned media. After two washes with cold phosphate-buffered saline (PBS), cells were resuspended in Annexin V binding buffer (0.01M HEPES, 0.14M NaCl, 2.5 mM $CaCl_2$) and passed through a 30 μm cell strainer to generate single-cell suspensions. A staining solution containing Cy5.5-conjugated Annexin V (2.5μL per test, BD Biosciences, #559925) and PI solution (2.5 μL per test, Invitrogen, #00-6990-50) was used to stain cells. After a 15-min incubation in the dark, stained cells were analyzed with a BD FACS Canto analyser. Positive controls for each staining were included in each repeat for color compensation. FlowJo V10.6.2 was used for gating and analysis.

Colony formation assay

Suspensions of OVSAHO cells were passed through a 40μm cell strainer (Corning) to generate single-cell suspensions and seeded in 6-well plates at a density of 3000 cells per well. Cells were allowed to grow for five days to form small colonies before drug treatment for 48 or 72 h. Culture media was refreshed every 2–3 days until 16 days post-seeding. On day 16, colonies were fixed in ice-cold methanol for 10 min and stained with 0.5% crystal violet (in 20% methanol) for another 10 min, washed and dried overnight. Plates were imaged using a scanner, and the Fiji V2.0.0 was used to count colonies.

Cell cycle analysis

In the last 60 min of drug treatment, cells were incubated with 10 μM BrdU and 200 μM IdU sequentially for 30 min each. Three washes with lukewarm PBS were included between BrdU and IdU labeling. Cells were detached by trypsinization and washed twice with PBS, and fixed in 70% ethanol at 4°C overnight. The next day, 2M HCl with 0.5% Tx-100 was added for 30 min with agitation to denature chromosomes. Then, cells were washed with 0.1M NaB_4O_7 (pH 8.5) for 5 min to neutralize residue HCl, followed by blocking with 1% BSA in PBS with 0.2% Tween 20 for 30 min. Incorporated BrdU and IdU were probed with mouse anti-BrdU (1:25 in blocking buffer, BD347580) and AF488-conjugated goat-*anti*-mouse antibody (1:100 in blocking buffer, Invitrogen, #A11001) for 60 min each at room temperature. Two washes with blocking buffer were included between primary and secondary antibody incubations. Afterward, cells were incubated with FxCycle PI/RNase staining solution (Invitrogen, #F10797) for 15 min in the dark. Finally, stained cells were analyzed on a BD FACS Canto analyser, and data were analyzed using Flowjo V10.6.2.

DNA fiber analysis

Cells were pulse-labeled with 10 μM BrdU and 200 mM IdU in the same way as the cell cycle analysis. Approximately 2000 cells were spotted on a SuperFrost slide (2000/2 μL/spot, 2 spots/slide). The drop was allowed to dry for 5 min and immediately mixed with 7 μL of lysis buffer (200 mM Tris-HCl, pH 7.5, 50 mM EDTA, and 0.5% SDS) to release DNA from cells. After airdrying for five to 7 min, slides were tilted at 15°–30°, enabling the DNA mixture to run down the slide slowly. Next, slides were dried for 30 min, fixed (in 75% methanol and 25% acetic acid) and dried for another 30 min. Dried DNA spreads were briefly rinsed with distilled water and immersed in 2.5M HCl for 1 h to denature DNA. After two PBS washes, slides were blocked in the blocking buffer (1% BSA in PBS with 0.1% Tween 20) for 1 h. BrdU was probed by incubating slides with rat anti-BrdU antibody (1:50, Abcam, #ab6326) for 90 min, followed by two PBS washes, one wash with blocking buffer, and then 1-h incubation with AF647-conjugated goat anti-rat antibody (1:100, Invitrogen, #A21247) in the dark. Slides were washed and left in PBS overnight before IdU labeling. The next day, IdU was detected by 1-h incubation of mouse anti-BrdU antibody (for IdU detection, 1:50, #BD347580) and 1-h incubation of AF488-conjugated goat anti-mouse antibody (1:100, Invitrogen, #A11001). After rinsing away excess antibodies, slides were mounted with Fluoromount-G (Invitrogen, #00-4958-02). Slides were imaged using the Aurox laser-free confocal microscope within 48 h. DNA track length was manually measured using Fiji V2.0.0.

Immunofluorescence analysis

Experiments in 96 well plates were washed once with PBS and fixed with 4% formaldehyde (Fisher Scientific, #11586711) for 15 min. After removing formaldehyde and two PBS washes, cells were permeabilized with 0.1% Triton X-100 (Sigma-Aldrich, #T8787) in PBS for 20 min, before blocking in 1% BSA and 2% FBS in PBS for 60 min. Cells were incubated with mouse anti-γH2AX antibody (1:500, Sigma-Aldrich, #05–636) overnight at 4°C, followed by three PBS washes. Next, cells were incubated with AF488-conjugated goat anti-mouse antibody (1:500, Invitrogen, #A11001) and DAPI (1:1000 in blocking buffer, Sigma-Aldrich, #D9542) for 2 h at room temperature. Stained cells were washed with PBS three times and 200 μL and imaged in 200 μL PBS. IN Cell Analyzer 1000 (GE Healthcare, UK) was used for imaging using a 20X objective. A minimum of 16 fields per well were acquired and CellProfiler (V3.1.8.) was used for image analysis.

Data availability

The *DCAF15* copy number variation and mRNA expression data in serous ovarian cancer patients were generated by the TCGA Research Network (PanCancer Atlas) and downloaded from the cBioPortal (https://www.cbioportal.org). The CTD[2] Drug sensitivity data in ovarian cancer cell lines and *DCAF15* expression data were downloaded from the DepMap (https://depmap.org/portal/). The

alternative splicing data included for systematic literature analysis were downloaded from online versions of the original publications. RNAseq data generated in this manuscript has been uploaded to the NCBI Gene Expression Omnibus and are accessible through GEO Series accession number GSE223011.

QUANTIFICATION AND STATISTICAL ANALYSIS

Statistical analyses were performed by GraphPad Prism 9. For data with normal distribution, the Student's t-test was used for statistical analysis between two groups. One-way ANOVA and multiple comparisons test were used for analysis among three or more groups. Two-way ANOVA and multiple comparisons test were used when there were three or more groups with two factors. For non-parametric data, Kruskal-Wallis test and multiple comparisons test were used. Statistical significance for *in vitro* data were defined as ns = not significant, *$p < 0.05$, **$p < 0.01$, ***$p < 0.001$, ****$p < 0.0001$. The Log rank (Mantel-Cox) test with Bonferroni-corrected significance threshold (0.0083) was used to calculate statistical differences between surviving proportions in the animal studies. Statistical details are specified in the figure legends.